Physics of the Earth and Planetary Interiors 225 (2013) 41–67

Contents lists available at ScienceDirect

Physics of the Earth and Planetary Interiors

journal homepage: www.elsevier.com/locate/pepi

Global correlations between maximum magnitudes of subduction zone interface thrust earthquakes and physical parameters of subduction zones

W.P. Schellart [a,*], N. Rawlinson [b]

[a] School of Geosciences, Monash University, Melbourne, VIC 3800, Australia
[b] Research School of Earth Sciences, The Australian National University, Canberra, ACT 0200, Australia

ARTICLE INFO

Article history:
Received 31 December 2012
Received in revised form 13 August 2013
Accepted 2 October 2013
Available online 14 October 2013
Edited by G. Helffrich

Keywords:
Earthquake
Moment magnitude
Subduction
Stress
Rupture
Asperity

ABSTRACT

The maximum earthquake magnitude recorded for subduction zone plate boundaries varies considerably on Earth, with some subduction zone segments producing giant subduction zone thrust earthquakes (e.g. Chile, Alaska, Sumatra–Andaman, Japan) and others producing relatively small earthquakes (e.g. Mariana, Scotia). Here we show how such variability might depend on various subduction zone parameters. We present 24 physical parameters that characterize these subduction zones in terms of their geometry, kinematics, geology and dynamics. We have investigated correlations between these parameters and the maximum recorded moment magnitude (M_W) for subduction zone segments in the period 1900–June 2012. The investigations were done for one dataset using a geological subduction zone segmentation (44 segments) and for two datasets (rupture zone dataset and epicenter dataset) using a 200 km segmentation (241 segments). All linear correlations for the rupture zone dataset and the epicenter dataset ($|R| = 0.00–0.30$) and for the geological dataset ($|R| = 0.02–0.51$) are negligible-low, indicating that even for the highest correlation the best-fit regression line can only explain 26% of the variance. A comparative investigation of the observed ranges of the physical parameters for subduction segments with $M_W > 8.5$ and the observed ranges for all subduction segments gives more useful insight into the spatial distribution of giant subduction thrust earthquakes. For segments with $M_W > 8.5$ distinct (narrow) ranges are observed for several parameters, most notably the trench-normal overriding plate deformation rate ($v_{OPD\perp}$, i.e. the relative velocity between forearc and stable far-field backarc), trench-normal absolute trench rollback velocity ($v_{T\perp}$), subduction partitioning ratio ($v_{SP\perp}/v_{S\perp}$, the fraction of the subduction velocity that is accommodated by subducting plate motion), subduction thrust dip angle (δ_{ST}), subduction thrust curvature (C_{ST}), and trench curvature angle (α_T). The results indicate that $M_W > 8.5$ subduction earthquakes occur for rapidly shortening to slowly extending overriding plates ($-3.0 \leqslant v_{OPD\perp} \leqslant 2.3$ cm/yr), slow trench velocities ($-2.9 \leqslant v_{T\perp} \leqslant 2.8$ cm/yr), moderate to high subduction partitioning ratios ($v_{SP\perp}/v_{S\perp} \leqslant 0.3–1.4$), low subduction thrust dip angles ($\delta_{ST} \leqslant 30°$), low subduction thrust curvature ($C_{ST} \leqslant 2.0 \times 10^{-13}$ m^{-2}) and low trench curvature angles ($-6.3° \leqslant \alpha_T \leqslant 9.8°$). Epicenters of giant earthquakes with $M_W > 8.5$ only occur at trench segments bordering overriding plates that experience shortening or are neutral ($v_{OPD\perp} \leqslant 0$), suggesting that such earthquakes initiate at mechanically highly coupled segments of the subduction zone interface that have a relatively high normal stress (deviatoric compression) on the interface (i.e. a normal stress asperity). Notably, for the three largest recorded earthquakes (Chile 1960, Alaska 1964, Sumatra–Andaman 2004) the earthquake rupture propagated from a zone of compressive deviatoric normal stress on the subduction zone interface to a region of lower normal stress (neutral or deviatoric tension). Stress asperities should be seen separately from frictional asperities that result from a variation in friction coefficient along the subduction zone interface. We have developed a global map in which individual subduction zone segments have been ranked in terms of their predicted capability of generating a giant subduction zone earthquake ($M_W > 8.5$) using the six most indicative subduction zone parameters ($v_{OPD\perp}$, $v_{T\perp}$, $v_{SP\perp}/v_{S\perp}$, δ_{ST}, C_{ST} and α_T). We identify a number of subduction zones and segments that rank highly, which implies a capability to generate $M_W > 8.5$ earthquakes. These

* Corresponding author. Tel.: +61 3 9905 1782; fax: +61 3 9905 4903.
E-mail address: wouter.schellart@monash.edu (W.P. Schellart).

http://dx.doi.org/10.1016/j.pepi.2013.10.001

include Sunda, North Sulawesi, Hikurangi, Nankai-northern Ryukyu, Kamchatka-Kuril-Japan, Aleutians-Alaska, Cascadia, Mexico-Central America, South America, Lesser Antilles, western Hellenic and Makran. Several subduction segments have a low score, most notably Scotia, New Hebrides and Mariana.

1. Introduction

At subduction zones oceanic lithosphere is recycled back into the Earth's mantle. The process of subduction is largely driven by subducted slabs of oceanic lithosphere, which are denser than the ambient mantle and are thus pulled downward by gravity (Elsasser, 1971; Forsyth and Uyeda, 1975; Hager, 1984; Davies and Richards, 1992). The potential energy that is released during sinking is used primarily to drive flow in the mantle, to move and deform the tectonic plates, and to deform the slab. Part of this potential energy is also used to overcome resistance at the subduction zone fault plate boundary, where part of the energy is released during interplate subduction zone thrust earthquakes.

Since the advent of plate tectonic theory it was recognized that subduction zones differ in many aspects that relate to their geometry, geology, physics and chemistry. At different subduction zones around the globe one might find differences in the age of the downgoing plate, nature of the overriding plate (continental/oceanic), overriding plate topography, overriding plate strain (extension/shortening), trench kinematics, subduction rate, subduction accretion/erosion rate, arc volcanism, slab dip angle, slab length, slab depth and trench curvature (e.g. Karig et al., 1976; Molnar and Atwater, 1978; Jarrard, 1986; Gudmundsson and Sambridge, 1998; Clift and Vannucchi, 2004; Heuret and Lallemand, 2005; Schellart, 2008). Similarly, it has been recognized that different subduction zones show differences in seismic behavior (e.g. Uyeda and Kanamori, 1979; Ruff and Kanamori, 1980; Peterson and Seno, 1984; Ruff, 1989; Pacheco et al., 1993; Stein and Okal, 2007). For example, several subduction zone segments have produced exceptionally large earthquakes in the last ~70 yr with moment magnitude $M_W \geqslant 9.0$, e.g. Alaska, Chile, Sumatra and Japan, while others have not, e.g. Scotia, New Hebrides and Mariana (Fig. 1). This could potentially be related to the relatively short period of global instrumental observations (McCaffrey, 1997, 2008; Stein and Okal, 2007), but it is also possible that there are essential physical ingredients that subduction zones require to be capable of producing giant earthquakes.

Numerous previous works have investigated the potential dependence between subduction zone thrust earthquake magnitude and various subduction zone parameters, including subducting plate age, subduction rate, sediment subduction, downdip extent of seismogenic zone, forearc structure, overriding plate velocity and overriding plate stress regime (e.g. Kelleher et al., 1974; Uyeda and Kanamori, 1979; Ruff and Kanamori, 1980; Peterson and Seno, 1984; Jarrard, 1986; Ruff, 1989; Pacheco et al., 1993; McCaffrey, 1993, 1997; Scholz and Campos, 1995; Llenos and McGuire, 2007; Stein and Okal, 2007; Heuret et al., 2011). In these previous works data are plotted for somewhat subjectively defined subduction zone segments, where the limits of such segments have some geological/structural/geometrical basis (e.g. aseismic ridge subduction, cusp, overriding plate nature) or can be somewhat arbitrary (such as for several South American segments). It is clear that the statistical correlation analyses performed in such studies are influenced by the choices of subduction zone segmentation.

In this paper we present a global investigation to test the dependence of the maximum subduction zone interplate thrust earthquake moment magnitude (M_W) on 24 subduction zone parameters. We test such dependence for all active subduction zones on Earth (23), which have been segmented into a total of 241 trench segments, each with a 200 km trench-parallel extent. Such segmentation into equal-length subduction segments gives equal weighing to each segment in the statistical analysis. For completeness, we also make such investigations using a geological subduction zone segmentation (total of 44 segments for 23 subduction zones), which is more in accordance with the previous works cited above. The 24 parameters are related to subduction zone geometry, kinematics, dynamics and geology. Our work shows that all the parameters have low or negligible correlations with M_W that are, with the exception of one, all statistically insignificant at 95% confidence level. Nevertheless, it will be demonstrated that very large subduction thrust earthquakes ($M_W > 8.5$) have only been observed under specific physical conditions with relatively narrow ranges for overriding plate deformation rate, trench migration velocity, subduction partitioning, subduction thrust dip angle, trench curvature angle and subduction thrust curvature. The relevance of these physical conditions can be explained in the framework of the physical parameters that quantify M_W. These findings provide new understanding as to why certain subduction zone segments have produced $M_W > 8.5$ earthquakes, which ones have the potential to produce them in the future, and which ones are not likely to produce them in the future. The findings also provide new understanding as to the occurrence and lateral rupture propagation of the three largest recorded earthquakes on Earth, namely the 1960 M_W 9.5 Chile earthquake, the 1964 M_W 9.2 Alaska earthquake and the 2004 M_W 9.1–9.3 Sumatra–Andaman earthquake.

2. Methods

2.1. Subduction zone parameters

In this paper we investigate the correlation between the maximum moment magnitude (M_W) for subduction zone interplate thrust earthquakes and 24 physical parameters of subduction zone characteristics. We have investigated 23 mature subduction zones in terms of subduction earthquakes and values for the 24 parameters. For several subduction zones, including Cyprus, Betic-Rif, Venezuela and South Shetland, the Wadati–Benioff zone is not accurately defined and/or subduction zone interface thrust earthquakes have not been recorded or could not be identified with confidence due to uncertainty in the subduction zone thrust geometry. This leaves us with 19 subduction zones for which the magnitudes, velocities, rates and values for the parameters were calculated (Fig. 1).

The correlations have been investigated using two different approaches that differ in the way that the 19 active subduction zones have been segmented. In one approach (referred to as the geological approach), the 19 subduction zones were divided into subduction zone segments based in particular on the geometrical characteristics of trench curvature (i.e. arcs), the nature of the overriding plate (continental or oceanic) or the presence of aseismic ridges/plateaus at the trench, resulting in a total of 40 segments. Narrow subduction zones (e.g. Scotia) are mostly represented by one data-point, while wide subduction zones (e.g. South America) are divided into 2–6 segments. In the other approach (in our view physically the most meaningful), each of the 19 subduction zones was divided into individual trench segments with a length of 200 km, resulting in a total of 228 subduction

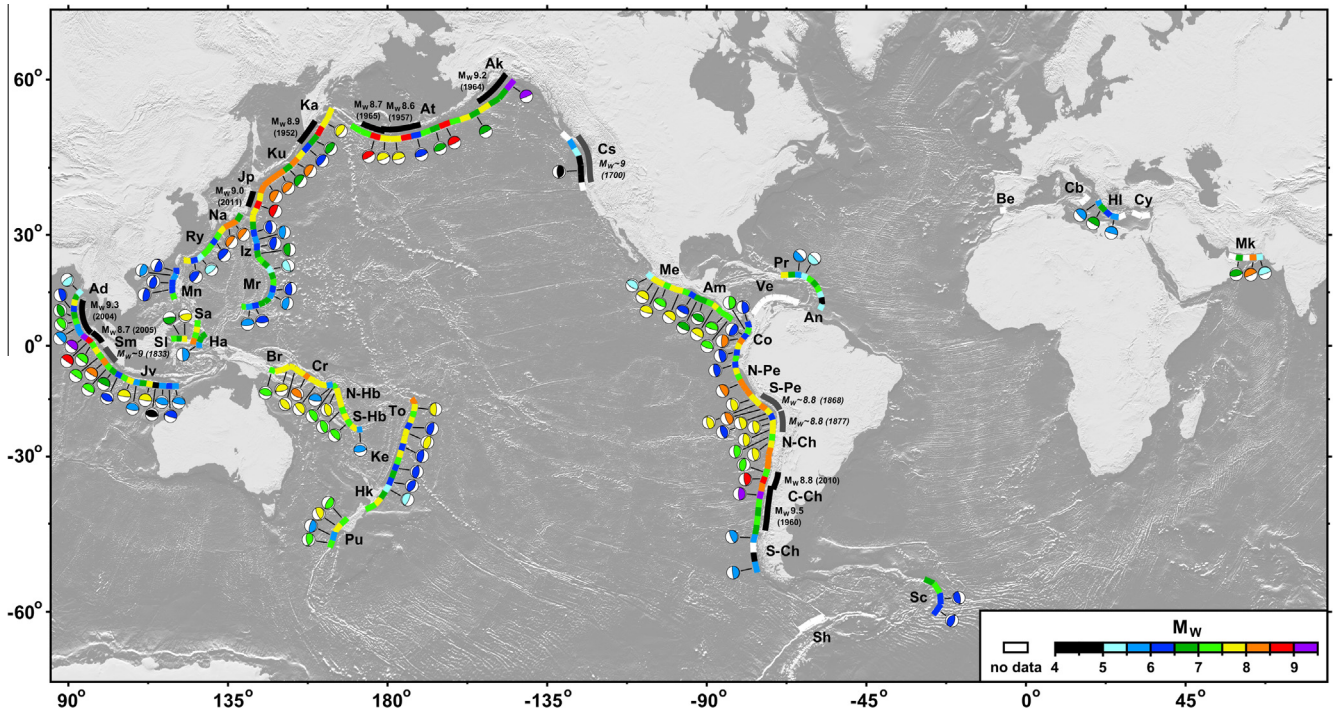

Fig. 1. Global map showing the location of the active subduction zones. Subduction zones have been divided into ~200 km segments as indicated by the colored line segments. Color indicates the maximum subduction zone thrust earthquake recorded in that segment in the period 1900–June 2012. For a large number of segments a focal mechanism has been plotted as obtained from the GCMT catalog or from published material (see Section 2). The map also shows the trench-parallel rupture extent of the largest earthquakes ($M_W > 8.5$) whose rupture extent overlaps with multiple trench segments (thick black lines for recorded earthquakes since 1900 and thick grey lines for four "historic" earthquakes before 1900). Numbers indicate the M_W value, while the year of the earthquake is in brackets (recorded earthquakes in bold and "historic" earthquakes in bold italic). Subduction zone segments: Ad – Andaman; Ak – Alaska; Am – Central America; An – Lesser Antilles; At – Aleutian; Be – Betic-Rif; Bl – Bolivia; Br – New Britain; C-Ch – Central Chile; Cb – Calabria; Co – Colombia; Cr – San Cristobal; Cs – Cascadia; Cy – Cyprus; Ha – Halmahera; Hk – Hikurangi; Hl – Hellenic; Iz – Izu-Bonin; Jp – Japan; Jv – Java; Ka – Kamchatka; Ke – Kermadec; Ku – Kuril; Me – Mexico; Mk – Makran; Mn – Manila; Mr – Mariana; N-Ch – North Chile; N-Hb – North New Hebrides; N-Pe – North Peru; Na – Nankai; Pr – Puerto Rico; Pu – Puysegur; Ry – Ryukyu; S-Ch – South Chile; S-Hb – South New Hebrides; S-Pe – South Peru; Sa – Sangihe; Sc – Scotia; Sh – South Shetland; Sl – North Sulawesi; Sm – Sumatra; To – Tonga; Ve – Venezuela.

segments. We emphasize that our rationale for the 200 km segmentation is not based on the segment size of the different earthquake ruptures (which is highly variable). Our 200 km segmentation is done to properly characterize the trench-parallel variability in magnitude of each of the physical parameters for the active subduction zones on Earth. Most of the 24 physical parameters are not constant along individual subduction zones, nor for individual arc-shaped segments of individual subduction zones. A geological segmentation does not capture the physical reality of the trench-parallel variability of individual parameters, while our 200 km segmentation does. Considering that we want to give equal weighing to all of our subduction zone segments (such that our statistical investigations are justified), it is most reasonable to make them all of equal length. We have chosen a 200 km segmentation such that the segments are not larger than the smallest subduction zones, such as Betic-Rif with ~250 km and Calabria with ~300 km. Furthermore, from a practical point of view, they should be larger than the thickness of the oldest oceanic lithosphere, which is ~95–106 km thick (Stein and Stein, 1992; McKenzie et al., 2005), because trench segments that are smaller than the thickness of the subducting oceanic lithosphere will show very similar values compared to neighboring trench segments, and with a smaller trench segment size a larger number of segments will have no data for M_W.

The 24 physical parameters that have been investigated are listed in Table 1 and most are illustrated in Fig. 2. They are meant to cover the broad range of geometric, kinematic, dynamic and geological parameters of subduction zones. Because of this several parameters are not fully independent. This is indicated by the correlation coefficients (R) for parameter sets obtained from least squares linear regression analysis. Parameters with the highest interdependence include $v_{OPD\perp}$ and OPSC ($R = 0.70$), $v_{OPD\perp}$ and $v_{T\perp}$ ($R = 0.66$), $v_{S\perp}$ and $v_{C\perp}$ ($R = 0.56$), δ_{ST} and δ_S ($R = 0.62$), $v_{A\perp}$ and T_{TS} ($R = 0.66$), $v_{A\perp}$ and T_{SS} ($R = 0.55$), T_{TS} and T_{SS} ($R = 0.89$), C_T and C_{ST} ($R = 0.94$), C_T and $|\alpha_T|$ ($R = 0.91$), C_{ST} and $|\alpha_T|$ ($R = 0.80$), L_{UMS} and D_{UMS} ($R = 0.88$), and L_{UMS} and F_{Bu} ($R = 0.76$). For completeness we present the results of all 24 parameters in Figs. 3 and 4.

For all the parameters that are velocities and rates ($v_{OPD\perp}$, $v_{SP\perp}$, $v_{OP\perp}$, $v_{T\perp}$, $v_{S\perp}$, $v_{C\perp}$, $v_{A\perp}$) the trench-normal component was calculated. From all the 24 parameters only $v_{OP\perp}$, $v_{SP\perp}$, $v_{T\perp}$ and $v_{SP\perp}/v_{S\perp}$ are dependent on the choice of global reference frame. Here we use the Indo-Atlantic moving hotspot reference frame from O'Neill et al. (2005) as our preferred frame of reference, because in this reference frame subduction kinematics is most in agreement with observed upper mantle slab structure and lower mantle high-velocity anomalies (Schellart, 2011; Schellart and Spakman, 2012), and it fits best with plate kinematics and energy minimization arguments (Schellart et al., 2008). Furthermore, global plate motion studies indicate that plate motions in Indo-Atlantic hotspot reference frames are generally in best agreement with the global asthenosphere anisotropy pattern below the interior of the plates (Kreemer, 2009; Conrad and Behn, 2010). We also briefly discuss results using the Pacific fixed hotspot reference frame from Gripp and Gordon (2002). We note that the Pacific hotspot frame gives significantly different plate and trench velocities at individual subduction zones (see Schellart et al., 2008), but the parameter correlations are low as for the Indo-Atlantic hotspot frame, while the ranges are generally larger (see Table 2). The hotspot reference

Table 1
24 Subduction zone parameters.

Parameter	Units	Explanation
$v_{OPD\perp}$	[cm/yr]	Trench-normal overriding plate deformation rate (Fig. 2a) (extension/spreading is positive, shortening is negative); Most rates were calculated using geodetically defined Euler parameters as summarized in Schellart (2008)
OPSC		Overriding plate strain class (Fig. 2a) (based on Jarrard, 1986): −3 = highly compressive; −2 = intermediately compressive; -1 = mildly compressive; 0 = neutral; 1 = mildly extensional; 2 = moderately to highly extensional; 3 = spreading; Data were extracted and updated from Schellart (2008)
$v_{A\perp}$	[cm/yr]	Trench-normal overriding plate accretion/erosion rate (Fig. 2b), which is the rate at which material is added to the overriding plate by accretion (positive) or removed from the overriding plate by erosion (negative); Compiled from Clift and Vannucchi (2004); For several subduction zones no data are available
$v_{SP\perp}$	[cm/yr]	Trench-normal subducting plate velocity (Fig. 2c); Trenchward motion is positive
$v_{OP\perp}$	[cm/yr]	Trench-normal overriding plate velocity (Fig. 2c); Trenchward motion is positive
$v_{T\perp}$	[cm/yr]	Trench-normal trench migration velocity (Fig. 2c), also often referred to as subduction hinge migration velocity or rollback velocity, where $v_{T\perp} = v_{OP\perp} + v_{OPD\perp} + v_{A\perp}$; Migration towards the subducting plate side (rollback) is positive
$v_{S\perp}$	[cm/yr]	Trench-normal subduction velocity (Fig. 2c), which is the velocity at which the subducting plate disappears into the mantle at the trench, i.e. $v_{S\perp} = v_{T\perp} + v_{SP\perp}$
$v_{C\perp}$	[cm/yr]	Trench-normal convergence velocity (Fig. 2c), which is the velocity of the subducting plate relative to the overriding plate, i.e. $v_{C\perp} = v_{SP\perp} + v_{OP\perp}$
$v_{SP\perp}/v_{S\perp}$		Subduction partitioning, which gives the fraction of the subduction velocity that is accommodated by trenchward subducting plate motion
A_{SP}	[Ma]	Subducting plate age (Fig. 2d), which is the age of the subducting plate at the trench; Data were obtained from Schellart (2008)
T_{TS}	[km]	Thickness of the trench sediments (Fig. 2b); Data were obtained from Clift and Vannucchi (2004) and Syracuse et al. (2010)
T_{SS}	[km]	Thickness of the subducted sediments (Fig. 2b); Data were obtained from Syracuse et al. (2010)
δ_{ST}	[°]	Subduction zone thrust dip angle (Fig. 2e), which is the dip angle of the subduction zone thrust from the trench down to 50 km depth; Values were calculated from the location of the trench (Bird, 2003) and the location of the 50 km isodepth contour for the subducted slab (Gudmundsson and Sambridge, 1998); For some subduction zones and segments no data are available
δ_S	[°]	Shallow slab dip angle (Fig. 2e), which is the dip angle of the slab as measured between 0 km and 125 km depth; Data were obtained from Schellart (2008); For some subduction segments no data are available
δ_D	[°]	Deep slab dip angle (Fig. 2e), which is the dip angle of the slab as measured between 125 km and 670 km depth; Data were obtained from Schellart (2008); For some subduction segments no data are available
D_{UMS}	[km]	Upper mantle slab tip depth (Fig. 2e), which is the depth of the slab tip in the upper mantle ($D_{UMS} \leqslant 670$ km); If the slab tip is in the lower mantle then $D_{UMS} = 670$ km; Data were obtained from Schellart et al. (2008)
L_{UMS}	[km]	Slab length (Fig. 2e), which is the upper mantle down-dip slab length, excluding horizontal slab segments located at the 670 km discontinuity; Values were calculated from δ_S, δ_D and D_{UMS}
W	[km]	Slab width (Fig. 2f), which is the trench-parallel extent of the slab; Data were obtained from Schellart et al. (2007, 2010)
D_{SE}	[km]	Distance to the closest lateral slab edge (Fig. 2f), which is the distance from the center of the trench segment to the closest lateral edge of the subducted slab; Data were obtained from Schellart (2008)
F_{Bu}	[N/m]	Upper mantle slab negative buoyancy force per meter trench length (Fig. 2c), which is the product of L_{UMS}, average slab thickness (which is related to slab age following the square root age law), average density contrast between slab and ambient upper mantle, and the gravitational acceleration ($g = 9.8$ m/s^2)
C_T	[m^{-2}]	Subduction zone trench curvature (Fig. 2f), where $C_T = 1/r^2$ and r is the radius of trench curvature
C_{ST}	[m^{-2}]	Subduction zone thrust curvature, which is the curvature of the subduction zone thrust plane (from the trench down to 50 km depth), where $C_{ST} = \sin(\delta_{ST})/r^2$
α_T	[°]	Trench segment curvature angle (Fig. 2g); Note that concave curvature towards the overriding plate is positive
$\lvert\alpha_T\rvert$	[°]	The absolute value of the trench segment curvature angle

frames were combined with the geodetic relative plate motion model from Kreemer et al. (2003), which is representative of present-day relative plate velocities.

2.2. Earthquake data

We have extracted our earthquake data for subduction zone thrust events from four earthquake catalogs (GCMT, PAGER-CAT, NEIC PDE and ISC) as well as from a number of publications on large subduction zone thrust events (Stauder, 1968; Kanamori, 1970a, 1972, 1976, 1977; Abe, 1972; Wu and Kanamori, 1973; Ando, 1975; Beck and Ruff, 1987; Beck and Christensen, 1991; Byrne et al., 1992; Okal, 1992; Johnson et al., 1994; Johnson and Satake, 1999; Yagi, 2004; Matsubara et al., 2005; López and Okal, 2006; Satake and Atwater, 2007; Lay et al., 2009, 2010; Beavan et al., 2010). The GCMT catalog contains a global set of earthquakes since 1976 with moment magnitude $M_W > 5.0$. We use this catalog for the period January 1976–June 2012, which lists 37,164 events. The PAGER CAT catalog is an earthquake database from the United States Geological Survey (USGS) that contains input from various catalogs (Allen et al., 2009), and spans the period 1900–December 2007 (with emphasis on earthquakes since 1973). Earthquakes with a magnitude greater than 5.5 are listed and it contains a total of 22,000 earthquakes. The NEIC PDE catalog is an earthquake database from the National Earthquake Information Center (NEIC) of the USGS starting from 1973. It includes worldwide events with magnitude >4.5 and we consider 431,789 earthquakes that are listed in the catalog between 1973 and June 2010. The ISC Bulletin is an earthquake database from the International Seismological Centre. We use data for the period 1904–July 2012, and consider a total of 55,584 events.

The issue of magnitude heterogeneity between catalogs due to the use of different datasets, methods of analysis and magnitude scales (e.g. Pacheco and Sykes, 1992; Engdahl and Villaseñor, 2002) can be significant, but in our study this effect is minimal due to the nature and origin of the catalogs we have chosen, our focus on large shallow subduction thrust earthquakes and the predominant use of M_W (193 out of 216 for the rupture zone dataset, see further below, with the remaining 23 being relatively small and having magnitudes of $\leqslant$7.8). We have found that estimates of M_W for this class of events experience little variation across the catalogs (generally not more than 0.1), and are not sufficient to influence our results. This is no doubt partly due to data inheritance (e.g. ISC draws on both NEIC PDE and GCMT), but also due to improvement of instrumentation (in both quality and distribution) and analysis techniques.

Another characteristic of the earthquake catalogs is that the quality and quantity of their entries has a strong dependence on the capabilities of the global (and in some cases regional) seismic networks that were available at the time. The value of a global network of seismometers was recognized as far back as 1895, just 6 yr after it was discovered that earthquakes could be detected at long

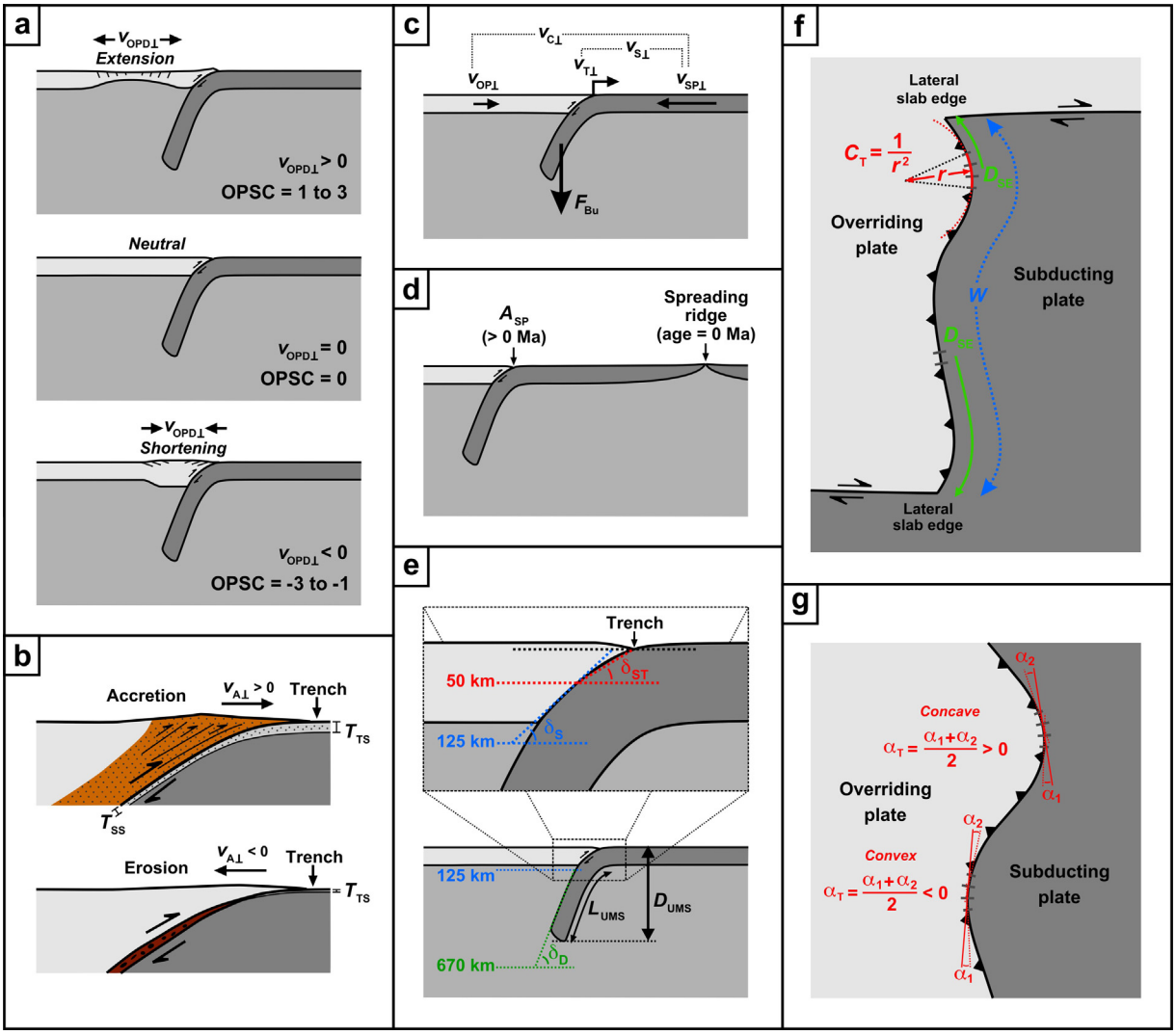

Fig. 2. Schematic diagrams illustrating most of the 24 subduction zone parameters that are investigated in relation to their potential influence on maximum recorded subduction zone thrust earthquake moment magnitude (M_W). (a) Trench-normal overriding plate deformation rate ($v_{OPD\perp}$) and overriding plate strain class (OPSC). (b) Trench-normal trench accretion rate ($v_{A\perp}$), trench sediment thickness (T_{TS}) and subducted sediment thickness (T_{SS}). (c) Trench-normal subducting plate velocity ($v_{SP\perp}$), trench-normal overriding plate velocity ($v_{OP\perp}$), trench-normal trench velocity ($v_{T\perp}$), subduction velocity ($v_{S\perp}$), convergence velocity ($v_{C\perp}$) and slab negative buoyancy force (F_{Bu}). Note that subduction partitioning is $v_{SP\perp}/v_{S\perp}$. (d) Subducting plate age at the trench (A_{SP}). (e) Subduction thrust dip angle (δ_{ST}), shallow slab dip angle (δ_S), deep slab dip angle (δ_D), upper mantle slab tip depth (D_{UMS}) and upper mantle slab length (L_{UMS}). (f) Slab width (W), lateral slab edge distance (D_{SE}) and trench curvature (C_T). Note that subduction thrust curvature C_{ST} is estimated as $C_{ST} = C_T \sin(\delta_{ST})$. (g) Trench curvature angle (α_T). Note that $|\alpha_T|$ is the absolute value of trench curvature.

distances (Agnew et al., 1976). Although the first network of standardized instruments was in place by 1898 (Dewey and Byerly, 1969), it wasn't until the early 1960s that a standardized network of high quality instruments came into existence in the form of the World-Wide Network of Standard Seismographs or WWNSS (Oliver and Murphy, 1971) with 120 continuously recording analog stations from 1967 onwards. In 1986, the Global Seismographic Network (GSN) was established to replace the by then obsolete WWNSS (Butler et al., 2004). GSN comprises some 150 high quality digital broadband stations that transmit their recordings in real time.

Given the above, it is clear that the quality and quantity of seismic data recorded today far exceeds that which was available prior to WWNSS, and that between the establishment of WWNSS and now, considerable improvements have been made. As such, earthquakes from the early 1900s will invariably be less accurately constrained and much more sparse than entries from the last 30–40 yr. Although this creates challenges for studies that seek to analyze patterns in global seismicity over time, it is worth noting that in our case, only the largest earthquakes from subduction zone regions are of interest, and these will almost always be better recorded and analyzed than smaller events.

We have searched the four earthquake catalogs for subduction zone thrust events using the following two search criteria: (1) The event must lie within the area of a polygon formed by the 200 km trench segment, the adjoining segment of the 50 km slab contour, and two lines that begin at each end of the trench segment and have equal angular distance between the trench segment and the adjoining trench segment at each end. We allow for a 15 km location error. The trench locations have been extracted from Bird (2003) and the 50 km slab contour locations have been extracted from Gudmundsson and Sambridge (1998). (2) The event must lie at a depth between 0.0 km and 50.0 km. For the GCMT catalog we have two additional search criteria: (3) The *T*-Axis of the focal solution must have a minimum plunge of 45 degrees, and *N*-axis plunge must not exceed 15°. (4) The maximum (strike) angle between the trench segment and the nodal planes of the focal solution must not exceed 30 degrees. The last two search criteria tend to eliminate most reverse events that are not subduction zone interface thrust events, as well as strike-slip events and normal

Table 2
Correlations and ranges for 24 subduction zone parameters (200 km datasets).

Parameter	n	Total range	Rupture zone dataset (RZD)				Epicenter dataset (ED)			
			R	Range for $M_W > 8.5$	% of total range	P	R	Range for $M_W > 8.5$	% of total range	P
$v_{OPD\perp}$	216	−3.2 to 15.0	−0.04	−3.0 to 2.3	29	0.003	−0.00	−3.0 to 0	16	0.011
OPSC	216	−3 to 3	−0.21	−3 to 1	67	0.000	−0.22	−3 to 0	50	0.011
$v_{A\perp}$	216	−0.5 to 0.6	−0.03	−0.3 to 0.6	82	0.256	−0.27	−0.3 to 0.6	82	0.653
$v_{SP\perp}$ (IA)	209	−3.6 to 9.3	0.26	1.0–8.0	55	0.010	0.28	1.5–8.0	50	0.143
$v_{OP\perp}$ (IA)	209	−5.9 to 6.7	0.03	−2.7 to 2.7	43	0.001	0.06	−1.0 to 2.7	30	0.022
$v_{T\perp}$ (IA)	216	−4.1 to 15.4	−0.02	−2.9 to 2.8	29	0.001	0.02	−2.8 to 2.8	29	0.086
$v_{S\perp}$	216	0.1–22.9	0.23	2.2–9.2	31	0.001	0.19	3.5–9.2	25	0.026
$v_{C\perp}$	209	−2.0 to −9.8	0.26	0.1–9.5	79	0.151	0.30	3.4–9.5	52	0.018
$v_{SP\perp}/v_{S\perp}$ (IA)	209	−2.5 to 6.2	0.05	0.3–1.4	13	0.001	0.06	0.4–1.2	10	0.016
A_{SP}	216	2–159	−0.13	11–134	78	0.003	−0.13	26–134	69	0.023
T_{TS}	201	0.3–6.0	0.11	0.6–5.0	77	0.000	−0.16	0.6–5.0	77	0.001
T_{SS}	201	0.1–3.4	0.20	0.3–2.6	70	0.000	−0.04	0.3–2.6	70	0.000
δ_{ST}	205	7–53	0.01	10–30	43	0.002	0.13	10–25	32	0.019
δ_S	216	10–72	−0.11	16–40	39	0.000	−0.07	16–40	39	0.072
δ_D	208	25–86	−0.15	29–79	82	0.091	−0.10	30–76	75	0.327
D_{UMS}	216	60–670	0.04	200–670	77	0.073	0.03	300–670	61	0.162
L_{UMS}	216	157–1674	0.17	299–1444	75	0.017	0.16	436–1397	63	0.115
W	216	500–7850	0.29	3400–7850	61	0.000	0.17	3400–7850	61	0.007
D_{SE}	216	100–3900	0.28	100–3300	84	0.300	0.25	100–3100	79	0.538
F_{Bu}	216	3.1×10^{12}–1.7×10^{14}	0.16	1.2×10^{13}–1.4×10^{14}	81	0.053	0.14	2.9×10^{13}–1.4×10^{14}	69	0.068
C_T	216	1.2×10^{-17}–5.2×10^{-12}	−0.22	6.9×10^{-17}–9.4×10^{-13}	18	0.014	−0.18	2.6×10^{-15}–3.2×10^{-13}	6	0.007
C_{ST}	205	2.7×10^{-18}–4.0×10^{-12}	−0.15	1.5×10^{-17}–2.0×10^{-13}	5	0.001	−0.10	7.0×10^{-16}–7.7×10^{-14}	2	0.004
α_T	216	−21.8 to 20.0	−0.18	−6.3 to 9.8	39	0.001	−0.21	−6.3 to 5.2	28	0.015
$\lvert\alpha_T\rvert$	216	0.0–21.8	−0.26	0.1–9.8	45	0.003	−0.20	0.6–6.3	26	0.007
$v_{SP\perp}$ (Pa)	209	−7.0 to 11.9	0.10	−0.5 to 11.3	62	0.034	0.16	2.0–11.3	49	0.030
$v_{OP\perp}$ (Pa)	209	−9.3 to 10.4	0.08	−4.2 to 4.1	42	0.000	0.04	−4.2 to 3.9	42	0.041
$v_{T\perp}$ (Pa)	216	−7.2 to 12.1	0.03	−6.0 to 4.4	54	0.005	0.02	−6.0 to 4.2	53	0.144
$v_{SP\perp}/v_{S\perp}$ (Pa)	209	−4.9 to 23.7	−0.03	−0.2 to 1.7	7	0.000	0.01	0.3–1.7	5	0.012

For an explanation of the 24 subduction zone parameters and their units see Table 1. Note that n is the number of data points, R is the correlation coefficient (calculated through least squares linear regression analysis), and P is the probability for all the earthquakes with $M_W > 8.5$ to fall by pure chance inside the range for $M_W > 8.5$. Further note that (IA) refers to the Indo-Atlantic moving hotspot reference frame from O'Neill et al. (2005), while (Pa) refers to the Pacific hotspot reference frame from Gripp and Gordon (2002). The rupture zone dataset contains mostly maximum M_W data points for epicenters of earthquakes located within polygons of individual trench segments (black diamonds in Fig. 3), but also data points for trench segments that overlap with the rupture area of giant earthquakes that cover multiple trench segments (red diamonds in Fig 3, which exclude trench segments with epicenter), which are assigned the M_W value of the giant earthquake. The epicenter dataset contains only maximum M_W data points for epicenters of earthquakes located within polygons of individual trench segments (black diamonds and green circles in Fig. 3).

events. From the discussion above it will be clear that those events extracted from the published literature and from the GCMT catalog have the highest probability of being a subduction zone thrust earthquake. For the earthquake data originating from the GCMT catalog and the published literature, the focal mechanism solutions have been checked to make sure these are (in all likelihood) indeed thrust events (see Fig. 1).

The earthquake data points in the dataset with the 200 km trench segments (Fig. 3) represent the maximum-recorded magnitude at each subduction zone segment. In case of a giant earthquake where the rupture area overlaps with more than one trench segment, we present two data points for those overlapping segments that do not contain the epicenter ($n = 25$): one data point that is assigned the M_W value of the giant earthquake (red diamonds in Fig. 3), and one data point that is assigned the maximum M_W of an earthquake with its epicenter located within that trench segment polygon (green circles in Fig. 3). The data points for the remaining trench segments ($n = 191$) are plotted as black diamonds in Fig. 3. As such, we define two datasets for the 200 km trench segments, namely a rupture zone dataset (RZD, black diamonds and red diamonds in Fig. 3) and an epicenter dataset (ED, black diamonds and green circles in Fig. 3).

The rupture zone and epicenter datasets each contain a maximum of 216 earthquake data points in Fig. 3. Most originate from the GCMT catalog and the published literature (97 and 43, respectively for RZD, 108 and 22 respectively for ED), giving a total of 140 (RZD) and 130 (ED). For these data points, their magnitude is relatively accurately determined and given in M_W, and the focal mechanisms are known. From the remaining data points (76 for RZD with 53 M_W, 8 M_S, 7 M_B and 8 unknown magnitude types, 86 for ED with 59 M_W, 11 M_S, 8 M_B and 8 unknown magnitude types) most are from the PAGER CAT catalog (69 in RZD and 78 in ED), with the remainder from the NEIC PDE catalog (6 in RZD and 6 in ED) and the ISC bulletin (1 in RZD and 2 in ED).

The dataset with the geologically defined trench segments contains a maximum of 37 data points in Fig. 4. We use the maximum-recorded magnitude (32 M_W, 4 M_S and 1 M_B) recorded within the geologically defined trench segment. In case the rupture area of a giant earthquake overlaps with more than one 200 km trench segment, then the value of the parameter is averaged for the overlapping trench segments. Note that in Figs. 3 and 4 we plot the small number of earthquakes with magnitude type other than M_W assuming that their numerical value is the same in M_W. Considering that their magnitudes are all relatively small ($\leqslant$7.8) this is reasonable. Also note that for some trench segments no earthquake data are available (see Fig. 1).

3. Results

3.1. Global variability in M_W at subduction zones

Fig. 1 shows the global distribution of subduction zones and their 200 km trench segments. Each trench segment is color coded to indicate the maximum recorded thrust earthquake that has

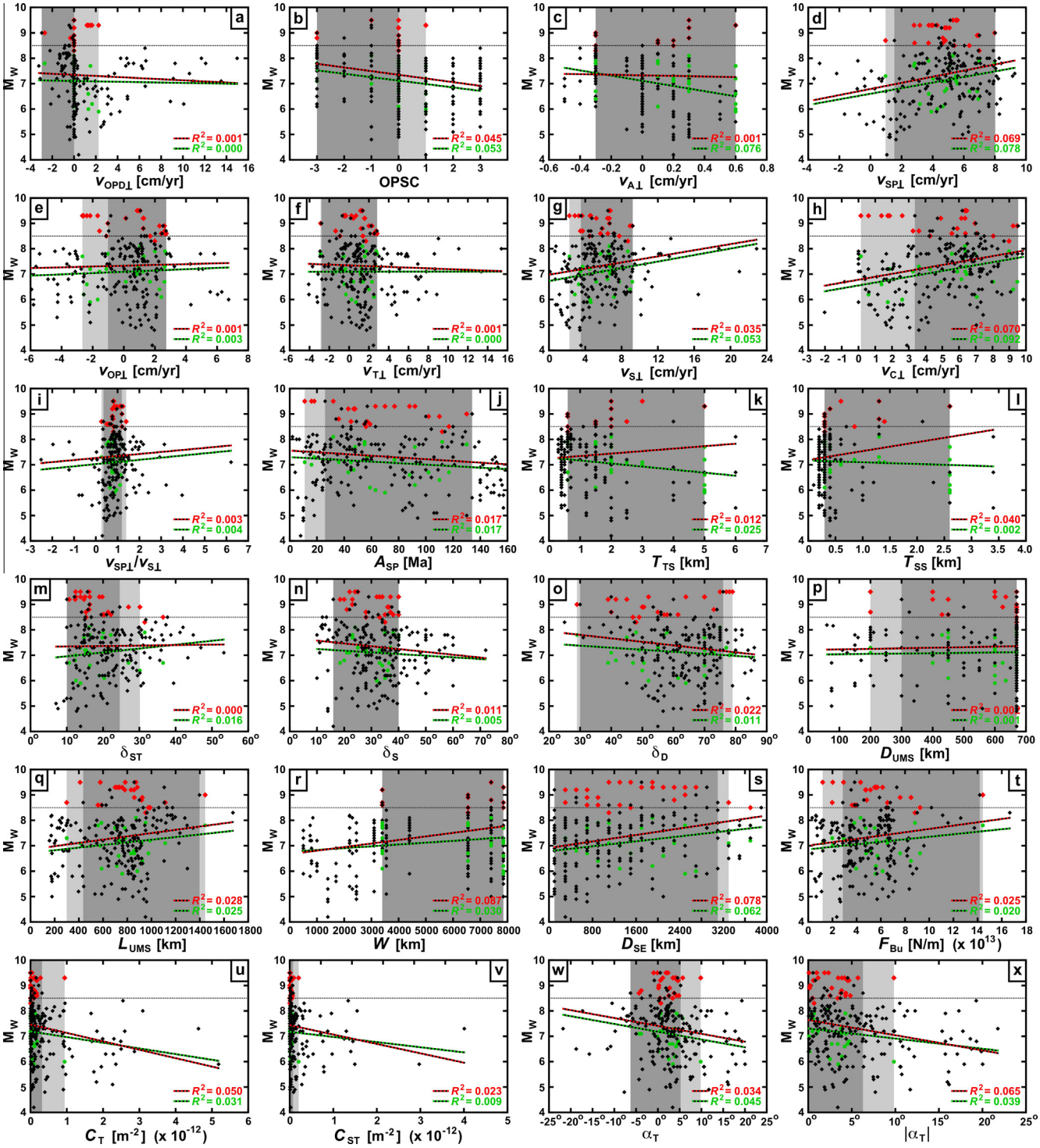

Fig. 3. Diagrams showing the dependence of subduction zone interplate thrust earthquake magnitude (maximum moment magnitude M_W) on 24 subduction zone parameters (see Table 1) for all active subduction zones on Earth, which have been subdivided into 200 km trench segments (n = 241). Note that earthquake data are available for 216 of the segments. The black diamonds represent maximum M_W data points for epicenters of earthquakes located within polygons of individual trench segments. In case of a giant earthquake where the rupture area overlaps with more than one trench segment, two data points are presented for those overlapping segments that do not contain the epicenter: one data point that is assigned the M_W value of the giant earthquake (red diamonds), and one data point that is assigned the maximum M_W of an earthquake with its epicenter located within that trench segment polygon (green circles). Due to this representation we define two datasets: (1) a "rupture zone dataset" (RZD) with black diamonds + red diamonds (with dashed red-black least squares linear regression best-fit line); and (2) an "epicenter" dataset (ED) with black diamonds + green circles (with dashed green-black least squares linear regression best-fit line) (see also Table 2). In each diagram the light grey area and dark grey area indicate the observed range of the particular parameter for earthquakes with M_W > 8.5 using the "rupture zone dataset". The dark grey area is exclusively for the observed range for earthquakes with M_W > 8.5 using the "epicenter dataset". R^2 is the coefficient of determination. Note that we have chosen the following magnitudes for the largest six earthquakes: Chile 1960 – M_W 9.5; Sumatra–Andaman 2004 – M_W 9.3; Alaska 1964 – M_W 9.2; Japan 2011 – M_W 9.0; Kamchatka 1952 – M_W 8.9; Chile 2010 – M_W 8.8. (For interpretation of the references to colour in this figure legend, the reader is referred to the web version of this article.)

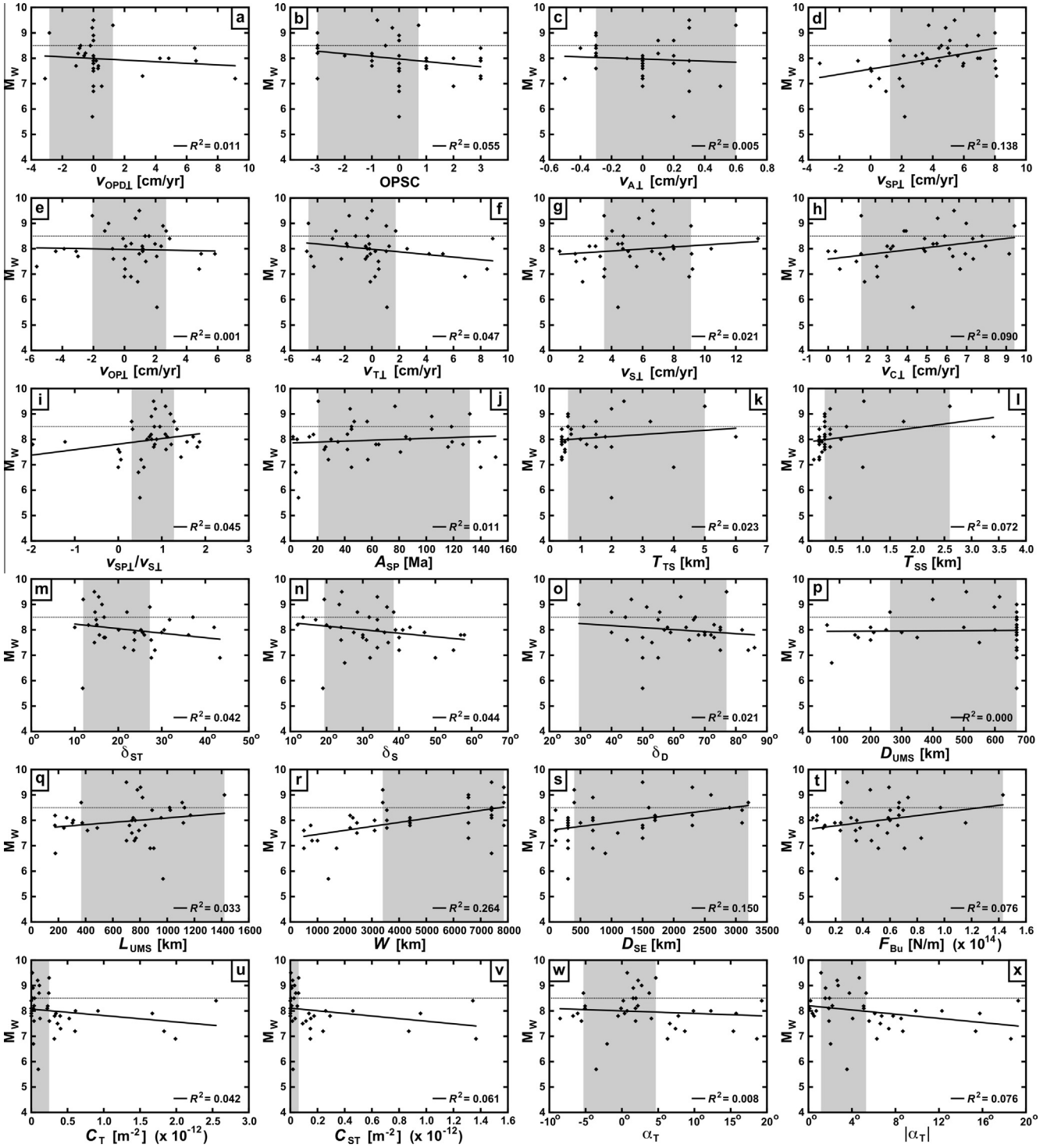

Fig. 4. Diagrams showing the dependence of subduction zone interplate thrust earthquake magnitude (maximum moment magnitude M_W) on 24 subduction zone parameters (see Table 1) for all active subduction zones on Earth. Subduction zones have been divided into one to six trench-parallel segments ($n = 44$) based on their geometry and geology (e.g. arc cusps, nature of overriding plate). Note that earthquake data are available for 37 of the segments. In each diagram the light grey area indicates the observed range of the particular subduction zone parameter for earthquakes with $M_W > 8.5$. Black line is least squares linear regression best fit line. R^2 is the coefficient of determination.

occurred there since 1900. The focal mechanism solution has been shown for those segments where such information is available. The figure also presents the rupture extent of those subduction zone thrust earthquakes with $M_W > 8.5$ that have occurred since 1950 in cases where it exceeds ~200 km. The figure shows a large variation in recorded maximum earthquake magnitude along individual subduction zones, such as South America, with a maximum M_W of 9.5 in central Chile (1960 earthquake) and maxima of only M_W 5.0–5.7 in southernmost Chile. Another notable example is the northwest Pacific subduction zone, where great and giant earthquakes have occurred along the Kamchatka, Kuril and Japan segments, while for the Izu-Bonin and Mariana segments all except the northernmost Izu Bonin segment have $M_W \leqslant 7.4$. There is also variability between subduction zones. Notably, several only show

low maxima in subduction earthquake magnitude with $M_W \leqslant 7.5$, including Scotia, Hellenic, Halmahera and Manila.

3.2. Subduction zone parameters and correlations with M_W

Fig. 3 and Table 2 show the correlations between the 24 subduction zone parameters and M_W for the 200 km trench segments recorded for the period 1900–June 2012 ($n = 201–216$). The correlation coefficients (R) and coefficients of determination (R^2) have been calculated through least squares linear regression analysis. The diagrams show that M_W is in the range 4.2–9.5. What is immediately apparent from the diagrams is the large amount of scatter of the data and the lack of a clear correlation for all the parameters. The large scatter is reflected in the low correlations ($R = -0.26$ to 0.29 for rupture zone dataset, RZD, and -0.27 to 0.30 for epicenter dataset, ED). This indicates that even for the parameters with the highest correlation (slab width for RZD with $R = 0.29$ and M_W increasing for increasing W, convergence velocity for ED with $R = 0.30$ and M_W increasing with increasing $v_{C\perp}$), the best-fit regression line can only explain 9% of the variance.

Fig. 4 and Table 3 show the correlations between the 24 subduction zone parameters and M_W for the geologically defined trench segments ($n = 33–37$). Here, M_W is in the range 5.7–9.5. For most parameters there is still considerable scatter of the data and a lack of correlation. However, several parameters do show a more moderate correlation. R is in the range -0.28 to 0.51 and R^2 is in the range 0.00–0.26. The parameter with the highest correlation is slab width ($R = 0.51$ with M_W increasing for increasing W), for which the best-fit regression line can explain 26% of the variance.

We have calculated confidence intervals for our correlations using Fisher's z. The highest correlation coefficient ($R = 0.51$) for W (geological dataset) is statistically significant at 97% confidence level. The second, third and fourth highest correlation coefficients for the geological dataset ($R = 0.39$ for D_{SE}, $R = 0.37$ for $v_{SP\perp}$ and $R = 0.30$ for $v_{C\perp}$) are statistically significant at 89% (D_{SE}) and 80% ($v_{SP\perp}$) and 69% ($v_{C\perp}$) confidence level. The highest correlation for the rupture zone dataset is $R = 0.29$ (again for W), which is statistically significant at 76% confidence level. The second, third and fourth highest correlation coefficients for the rupture zone dataset ($R = 0.28$ for D_{SE}, $R = 0.26$ for $v_{C\perp}$ and $R = 0.26$ for $v_{SP\perp}$) are statistically significant at 73% (D_{SE}) and 61% ($v_{C\perp}$) and 59% ($v_{SP\perp}$) confidence level. From these calculations we conclude that only the parameter W for the geological dataset (Fig. 4r) has a significant correlation with M_W, because its confidence level is at least 95%.

3.3. Subduction zone parameter ranges

The ranges of values observed for the 200 km trench segments that have experienced giant subduction zone thrust earthquakes are generally less than the total ranges for the 24 different parameters. Note that we define giant subduction zone thrust earthquakes as those with $M_W > 8.5$. The ranges for those trench segments with $M_W > 8.5$ ($n = 32$ for RZD and $n = 10$ for ED) with respect to the total range ($n = 201–216$) differ significantly for the 24 individual parameters, between 5% and 84% for RZD and between 2% and 82% for ED (Fig. 3, Table 2). Note that for simplicity, we will discuss in the remainder of the text only the ranges as observed for the rupture zone dataset RZD unless specified otherwise.

A number of physical parameters do not show a clear distinction between observed range for $M_W > 8.5$ and total observed range, including A_{SP}, $v_{C\perp}$, T_{TS}, D_{SE}, $v_{A\perp}$, T_{SS}, δ_D, L_{UMS}, OPSC, D_{UMS} and F_{Bu} with ranges for $M_W > 8.5$ being 67–82%. Parameters that show a moderate distinction between observed range for $M_W > 8.5$ and total observed range include W (61%) and $v_{SP\perp}$ (55%). Parameters that show a more clear distinction between observed range for $M_W > 8.5$ and total observed range include $v_{OPD\perp}$ (29%), $v_{OP\perp}$ (43%), $v_{T\perp}$ (29%), $v_{S\perp}$ (31%), $v_{SP\perp}/v_{S\perp}$ (13%), δ_{ST} (43%), δ_S (39%), C_T (18%), C_{ST} (5%), α_T (39%) and $|\alpha_T|$ (45%) (Table 2).

Table 3
Correlations and ranges for 24 subduction zone parameters (geological dataset).

Parameter	n	Total range	R	Range for $M_W > 8.5$	% of total range	P
$v_{OPD\perp}$	37	−3.1 to 9.1	−0.10	−2.8 to 1.3	33	0.230
OPSC	37	−3 to 3	−0.23	−3 to 0.7	62	0.084
$v_{A\perp}$	37	−0.5 to 0.6	−0.07	−0.3 to 0.6	82	0.678
$v_{SP\perp}$ (IA)	37	−3.3 to 8.1	0.37	1.3–8.0	59	0.110
$v_{OP\perp}$ (IA)	37	−5.6 to 5.8	−0.04	−2.1 to 2.7	41	0.142
$v_{T\perp}$ (IA)	37	−2.9 to 9.0	−0.22	−2.8 to 2.8	47	0.230
$v_{S\perp}$	37	0.7–13.4	0.15	3.5–9.1	44	0.048
$v_{C\perp}$	35	0–9.4	0.30	1.7–9.4	82	0.340
$v_{SP\perp}/v_{S\perp}$ (IA)	37	−2.0 to 1.9	0.21	0.3–1.3	25	0.064
A_{SP}	37	2–151	0.11	21–132	75	0.142
T_{TS}	33	0.4–6.0	0.15	0.6–5.0	79	0.030
T_{SS}	33	0.1–3.4	0.27	0.3–2.6	70	0.042
δ_{ST}	35	10–43	−0.21	12–27	46	0.053
δ_S	37	12–58	−0.21	19–39	42	0.036
δ_D	35	30–86	−0.14	30–77	84	0.534
D_{UMS}	37	60–670	0.02	263–670	67	0.182
L_{UMS}	37	174–1421	0.18	367–1421	84	0.230
W	37	500–7850	0.51	3400–7850	61	0.036
D_{SE}	37	100–3200	0.39	400–3200	90	0.085
F_{Bu}	37	3.1×10^{12}–1.4×10^{14}	0.28	2.4×10^{13}–1.4×10^{14}	85	0.085
C_T	37	1.4×10^{-16}–2.5×10^{-12}	−0.20	1.5×10^{-14}–2.5×10^{-13}	9	0.003
C_{ST}	35	4.7×10^{-18}–1.4×10^{-12}	−0.25	4.4×10^{-15}–6.1×10^{-14}	4	0.002
α_T	37	−8.5 to 19.3	−0.09	−5.3 to 4.7	36	0.026
$\lvert\alpha_T\rvert$	37	0.1–19.3	−0.28	1.2–5.3	22	0.004
$v_{SP\perp}$ (Pa)	37	−6.6 to 11.0	0.26	1.4–11.0	55	0.142
$v_{OP\perp}$ (Pa)	37	−8.4 to 8.3	−0.03	−4.0 to 0.8	29	0.142
$v_{T\perp}$ (Pa)	37	−6.3 to 10.3	−0.20	−5.8 to 2.2	48	0.230
$v_{SP\perp}/v_{S\perp}$ (Pa)	37	−4.0 to 2.9	0.16	0.3–1.6	19	0.036

For an explanation of the 24 subduction zone parameters and their units see Table 1. Note that n is the number of data points, R is the correlation coefficient (calculated through least squares linear regression analysis), and P is the probability for all the earthquakes with $M_W > 8.5$ to fall by pure chance inside the range for $M_W > 8.5$. Further note that (IA) refers to the Indo-Atlantic moving hotspot reference frame from O'Neill et al. (2005), while (Pa) refers to the Pacific hotspot reference frame from Gripp and Gordon (2002).

For each of the 24 physical parameters we have calculated the probability (P) that all the large events with $M_W > 8.5$ fall – by pure chance – within the selected narrow range of the total range (Tables 2 and 3). For RZD, the probabilities for all 24 parameters are between 0.00 and 0.30. For those parameters with narrow ranges ($v_{OPD\perp}$, $v_{OP\perp}$, $v_{T\perp}$, $v_{S\perp}$, $v_{SP\perp}/v_{S\perp}$, δ_{ST}, δ_S, C_T, C_{ST}, α_T, $|\alpha_T|$) the probabilities are very low ($P = 0.00$–0.01).

4. Discussion

4.1. Correlations between subduction zone parameters and M_W

From the data presented in Figs. 3 and 4 it is clear that none of the 24 parameters can individually explain the distribution of maximum observed M_W for individual subduction zone segments because of the low correlation coefficients for both 200 km datasets (RZD and ED) and for the geological dataset. The correlations for the geological dataset are generally somewhat higher than those for RZD and ED. Datasets RZD and ED give comparable (low to negligible) correlations.

The low correlations could potentially be explained due to the fact that accurate global recording of earthquake location and magnitude started only in the first half the 20th century (last ~60–110 yr), while the recurrence interval of very large earthquakes can be hundreds to thousands of years. For example, the recurrence interval for giant subduction zone earthquakes in northeast Japan is thought to be 800–1100 yr (Minoura et al., 2001), in agreement with the recent occurrence of the 2011 M_W 9.0 Japan earthquake.

Even if the lack in correlation is possibly related to the relatively short sampling period, it is worth discussing several parameters that have received much attention in the past, including subducting plate age, trench sediment thickness, overriding plate velocity, and slab dip angle (e.g. Uyeda and Kanamori, 1979; Ruff and Kanamori, 1980; Lamb and Davis, 2003; Stein and Okal, 2007; Heuret et al., 2011). Subducting plate age, trench sediment thickness and overriding plate velocity have very low correlations for all datasets with $|R| \leqslant 0.16$. Parameters related to subduction zone geometry (δ_{ST}, C_T, C_{ST} and $|\alpha_T|$) also show low correlations for all datasets ($|R| \leqslant 0.28$) but consistent trend lines (except δ_{ST}), weakly suggesting that giant earthquakes prefer relatively straight fault planes. Parameters that are linked to the state of normal stress on the subduction interface ($v_{OPD\perp}$ and OPSC) also give low correlations ($|R| \leqslant 0.23$) but consistent trend lines, weakly suggesting that giant earthquakes preferentially occur along subduction segments with a relatively high normal stress on the subduction zone interface. W and D_{SE} have some of the highest correlations with $R = 0.29$ (W) and $R = 0.28$ (D_{SE}) for the rupture zone dataset and $R = 0.51$ (W) and $R = 0.39$ (D_{SE}) for the geological dataset, giving a weak indication that giant earthquakes preferentially occur at wide subduction zones and away from slab edges.

Despite the generally very low correlations for the three datasets, it is concluded that several parameters do show correlations with M_W that are physically plausible and also consistent for the three datasets, including C_T, C_{ST} and $|\alpha_T|$, and $v_{OPD\perp}$, $v_{T\perp}$, W and D_{SE}. The datasets do provide additional insight into which parameters are more likely or less likely to have an influence on the maximum M_W at subduction zones. This can be deduced from comparing the range of values for each of the 24 parameters for those trench segments with $M_W > 8.5$ with the range of values for each parameter for all trench segments (Figs. 3 and 4, Tables 2 and 3). We will discuss these ranges in detail in Sections 4.2, 4.3 and 4.4. Note again that we will discuss in the remainder of the text only the ranges as observed for the rupture zone dataset (RZD) and not for the epicenter dataset (ED) or the geological dataset, unless specified otherwise.

4.2. Parameters with small (distinct) ranges for $M_W > 8.5$

Parameters that show a clear distinction between observed range for $M_W > 8.5$ (5–45%) and total observed range (100%) include $v_{OPD\perp}$, $v_{T\perp}$, $v_{OP\perp}$, $v_{SP\perp}/v_{S\perp}$, δ_{ST}, δ_S, C_T, C_{ST}, α_T, $|\alpha_T|$ and $v_{S\perp}$ (Table 2).

4.2.1. Overriding plate deformation rate and trench velocity

The parameters $v_{OPD\perp}$ and $v_{T\perp}$ have low values and small ranges for trench segments with $M_W > 8.5$, with $v_{OPD\perp} = -3.0$ to 2.3 cm/yr (29%) and $v_{T\perp} = -2.9$ to 2.8 cm/yr (29%) (Fig. 3a and f), while the probabilities for these distributions are low ($P = 0.00$, Table 2). The ranges suggest that giant subduction zone thrust earthquakes preferentially occur for those subduction zone segments for which the overriding plate is either relatively neutral, experiences minor extension or experiences shortening, while the trench is relatively stable with minor trench retreat or trench advance. Notably, giant earthquakes have not been recorded for trench segments that experience rapid trench retreat (e.g. Scotia, New Hebrides, Tonga, southwest Ryukyu), nor for those that experience considerable backarc extension/spreading (e.g. Scotia, Mariana, New Hebrides, Tonga, southwest Ryukyu). What is also notable is that for the epicenter dataset ED the range for $v_{OPD\perp}$ with $M_W > 8.5$ is −3.0 to 0 cm/yr, indicating that the epicenters of giant earthquakes have occurred only at trench segments with a neutral or shortening deformation regime in the overriding plate. Epicenters of giant earthquakes ($M_W > 8.5$) have not occurred at trench segments with an overriding plate that experiences extension. The probability for the $M_W > 8.5$ distribution in the epicenter dataset is low ($P = 0.01$, Table 2), implying a physical cause for the narrow distribution of $v_{OPD\perp}$ values for the epicenters of giant earthquakes.

Uyeda and Kanamori (1979) proposed that giant earthquakes occur for highly compressive subduction zones with significant backarc shortening, because only for such settings is there sufficient elastic strain energy accumulation to permit a large rupture. Since then others have also argued that a highly compressive stress regime is a requirement for the generation of giant earthquakes at subduction zones (e.g. Ruff and Kanamori, 1980; Ruff, 1989; Conrad et al., 2004; De Franco et al., 2008). In contrast, Heuret et al. (2011) argued that giant earthquakes occur for neutral overriding plates (no deformation), arguing that only a neutral stress regime at the subduction zone interface allows for large lateral propagation of the rupture.

The data presented in Fig. 3a show that the occurrence of giant earthquakes is more complex than previously proposed, ranging from highly compressive (deviatoric compression) with rapid overriding plate shortening rates (e.g. Japan, $v_{OPD\perp} = -3.0$ to −2.7 cm/yr) to mostly neutral (e.g. Alaska, $v_{OPD\perp} \approx 0$ for three segments, $v_{OPD\perp} = -0.3$ for easternmost segment) to mostly tensional (deviatoric tension) with slow overriding plate extension (e.g. Sumatra–Andaman, $v_{OPD\perp} = 1.2$–2.3 cm/yr for six segments, $v_{OPD\perp} = -0.4$ cm/yr for southernmost segment). What is noteworthy, is that the three largest recorded earthquakes (Chile 1960, Alaska 1964, Sumatra–Andaman 2004), which were all characterized by very large lateral rupture propagation (800–1300 km), all had their epicenter at a trench segment characterized by overriding plate shortening and a compressive deviatoric stress regime, with the rupture propagating towards the region characterized by a neutral or (mildly) extensional overriding plate and a neutral or tensional deviatoric stress regime (see Section 5.4 for more discussion).

As noted in the methods section, calculations of $v_{T\perp}$ depend on the choice of reference frame, with the Indo-Atlantic hotspot reference frame being our preferred frame. Calculations for $v_{T\perp}$ in the Pacific hotspot reference frame from Gripp and Gordon (2002) increase the range for $M_W > 8.5$ to −6.0 to 4.4 cm/yr (54%, Table 2).

4.2.2. Overriding plate velocity

The range for $v_{OP\perp}$ (−2.7 to 2.7 cm/yr) for $M_W > 8.5$ is smaller (43%) than the total range (−5.9 to 6.7 cm/yr) and it is centered on zero (Fig. 3e). The low values for $|v_{OP\perp}|$ and the centering on zero suggest that $M_W > 8.5$ earthquakes preferentially occur for subduction zones with a low $v_{OP\perp}$ and that within this relatively small range there is no preference for very large earthquakes to occur for either trenchward overriding plate motion or motion away from the trench. This is in contrast to previous suggestions that giant earthquakes preferentially occur at subduction segments for which the overriding plate moves trenchward at a high rate (e.g. Uyeda and Kanamori, 1979; Peterson and Seno, 1984; Conrad et al., 2004). We note, however, that our calculations of $v_{OP\perp}$ depend on the choice of reference frame, as explained in the Methods section, with the Indo-Atlantic hotspot reference frame having our preference, and thus that our conclusion from above depends on this choice. However, although our calculations for $v_{OP\perp}$ in the Pacific hotspot reference frame from Gripp and Gordon (2002) do make a difference in the distribution of data points, the range for $M_W > 8.5$ is comparable (42%) and is centered on zero (Table 2).

4.2.3. Subduction partitioning and subduction rate

The subduction partitioning parameter is closely related to the parameters $v_{T\perp}$ and $v_{SP\perp}$. The range for $v_{SP\perp}/v_{S\perp}$ ($M_W > 8.5$) is 0.3–1.4, which is 13% of the total range (−2.5 to 6.2) (Fig. 3i). The distribution of the data in Fig. 3i indicates that for most subduction segments experiencing giant earthquakes subduction is accommodated predominantly by trenchward subducting plate motion and not by trench retreat. In the Pacific hotspot reference frame the range for $v_{SP\perp}/v_{S\perp}$ ($M_W > 8.5$) is also small (7%).

The range for $v_{S\perp}$ ($M_W > 8.5$) is 2.2–9.2 cm/yr, which is 31% of the total range (0.1–22.9 cm/yr) (Fig. 3g). This indicates that those subduction segments have experienced giant earthquakes for which the subduction rate is moderately low to high. The fact that there are no recorded giant earthquakes at very high $v_{S\perp}$ ($\geqslant \sim 10$ cm/yr) is likely because the few subduction segments that experience very fast subduction do so due to very fast backarc opening and trench retreat (Tonga, New Hebrides, New Britain). Earthquakes with $M_W > 8.5$ have not been documented for these subduction zones, which can possibly be ascribed to the low normal stresses at the subduction interface due to rapid backarc opening and trench retreat (see Section 4.2.1). The fact that there are no recorded giant earthquakes for subduction segments with very low $v_{S\perp}$ ($<\sim 2$ cm/yr) can possibly be ascribed to the view that for slow subduction the recurrence time increases, so that in a finite time slow subduction zones are less likely to experience a giant earthquake (McCaffrey, 2008).

4.2.4. Subduction thrust dip angle and shallow slab dip angle

The subduction thrust dip angle δ_{ST} for subduction segments with $M_W > 8.5$ is 10–30°, which is 43% of the total range of values for δ_{ST} (7–53°) (Fig. 3m). This suggests that giant subduction zone thrust earthquakes preferentially occur for those segments that have a relatively gentle subduction thrust dip angle $\leqslant \sim 30°$. It has been argued before that giant earthquakes occur for gentle thrust dip angles and large downdip extent of the seismogenic zone (Kelleher et al., 1974; Uyeda and Kanamori, 1979; Lay et al., 1982), but it has also been argued that thrust dip angle and downdip extent of the seismogenic zone, which is closely related to δ_{ST}, play no role in the generation of giant earthquakes (Pacheco et al., 1993; Heuret et al., 2011). The current work suggests that a gentle subduction thrust dip angle ($\leqslant \sim 30°$) is a requirement for earthquakes with $M_W > 8.5$.

The shallow slab dip angle δ_S also shows a clear distinction between observed range for $M_W > 8.5$ and total observed range (39%) (Fig. 3n). For δ_S the dip angle is averaged over a depth range from the surface down to 125 km depth. There appears to be no physical reason as to why the local dip of the slab below the thrust interface seismogenic zone (i.e. below ∼50 km) should be of any relevance for predicting earthquake magnitude. However, δ_{ST} and δ_S are semi-dependent parameters and are moderately correlated ($R = 0.62$), suggesting that the narrow range observed for δ_S is mostly a consequence of the narrow range observed for δ_{ST}.

4.2.5. Trench curvature and subduction thrust curvature

The trench curvature C_T, subduction zone thrust curvature C_{ST}, trench curvature angle α_T and absolute value of the trench curvature angle $|\alpha_T|$ for subduction segments with $M_W > 8.5$ have narrow ranges (18%, 5%, 39% and 45%, respectively) (Fig. 3u–x). This suggests that giant subduction zone thrust earthquakes do not occur for those subduction zone segments that have a relatively strong trench curvature and subduction zone thrust curvature and a high $|\alpha_T|$. Notably, giant earthquakes have not been reported for strongly curved subduction zones such as Scotia, nor have giant earthquakes been reported to cross trench cusps with a strongly negative trench curvature angle ($\alpha_T \ll 0$). It thus appears that ruptures of giant earthquakes preferentially follow a relatively planar subduction zone thrust fault and that lateral rupture propagation will be halted in case of a strong increase in trench and thrust plane curvature.

4.3. Parameters with intermediate ranges for $M_W > 8.5$

Parameters that show a moderate distinction between observed range for $M_W > 8.5$ (55–61%) and total observed range (100%) include W and $v_{SP\perp}$ (Table 2).

4.3.1. Slab width

For earthquakes with $M_W > 8.5$, slab width ranges between 3100 and 7850 km, which is 61% of the total range (500–7850 km), suggesting that giant earthquakes preferentially occur at wide subduction zones (Fig. 3r). This is not entirely surprising, considering that wide subduction zones ($W > 3000$) account for the largest portion (∼36,250 km, ∼75%) of the global extent of subduction zones (∼48,200 km). This might partly explain why W shows the highest correlations of all parameters (Tables 2 and 3). Furthermore, M_W is mostly controlled by rupture length and amount of slip. It is clear that giant earthquakes with extreme rupture lengths (>600 km), such as the Sumatra–Andaman 2004, Chile 1960 and Alaska 1964 earthquakes, are not possible for the narrowest subduction zones with $W < 600$ km (e.g. Betic-Rif, Calabria, North Sulawesi, Halmahera). Nevertheless, such narrow subduction zones might still produce giant earthquakes with $M_W > 8.5$ in cases where the coseismic slip is very large (multiple tens of meters).

One can also argue from a mechanical point of view as to why relatively narrow subduction zones might be less likely to produce $M_W > 8.5$ earthquakes. Narrow subduction zones preferentially subduct through trench retreat as the slab pulls the subduction zone hinge and trench backward during slab rollback (Schellart et al., 2010). Such pull-back reduces the normal stress on the subduction zone interface, which, in combination with the mantle flow patterns excited by slab rollback, promotes rapid backarc extension such as found for the Scotia and Hellenic subduction zones (Schellart and Moresi, 2013; Duarte et al., 2013). Thus, narrow subduction zones are generally less capable of sustaining the buildup of large elastic strain energy at the subduction zone interface due to the low normal stress. It therefore appears plausible that narrow subduction zones preferentially release seismic energy through a relatively large number of relatively minor earthquakes. In contrast, wide subduction zones have a relatively stable subduction zone hinge, in particular in the center, which can sustain large

normal stresses (Schellart and Moresi, 2013) and thus the buildup of large elastic strain energy, which can be released in larger earthquakes.

It should be remembered, though, that, apart from slab width, there are several other factors that influence trench migration rate (e.g. slab length, plateau/aseismic ridge subduction, tearing resistance), such that not all narrow subduction zones retreat rapidly or show rapid backarc extension. It is thus likely that some relatively narrow subduction zones are capable of producing very large earthquakes. Indeed, the Cascadia subduction zone is relatively narrow (W = 1400 km), has a relatively neutral overriding plate (with minor shortening in the north and minor extension in the south), and is thought to have experienced an M_W ~9 earthquake in 1700 (Satake et al., 2003).

4.3.2. Subducting plate velocity

For $v_{SP\perp}$ the range (1.0–8.0 cm/yr) is moderately smaller (55%) than the total range (−3.6 to 9.3 cm/yr) (Table 2). The data in Fig. 3d suggest that earthquakes with $M_W > 8.5$ do not occur when $v_{SP\perp} < \sim 1$ cm/yr. Calculations for $v_{SP\perp}$ in the Pacific hotspot reference frame give a comparable range of 62%.

4.4. Parameters with large (indistinct) ranges for $M_W > 8.5$

Physical parameters that do not show a clear distinction between observed range for $M_W > 8.5$ (68–84%) and total observed range (100%) include A_{SP}, $v_{C\perp}$, $v_{A\perp}$, T_{TS}, T_{SS}, D_{SE}, δ_D, L_{UMS}, D_{UMS} and F_{Bu} (Table 2).

4.4.1. Subducting plate age

Our compilation shows that the range in A_{SP} is 11–134 Ma for $M_W > 8.5$, which is 78% of the total range of 2–159 Ma (Fig. 3j). This indicates that giant earthquakes can occur at subduction zones that consume very young to very old oceanic lithosphere. Earlier work (Ruff and Kanamori, 1980) found that subducting lithospheric age, in combination with subduction rate, correlates strongly with earthquake magnitude. The authors argued that the largest earthquakes occur at subduction zones that are characterized by rapid subduction of young lithosphere. The rationale was based on earlier conceptual models of the influence of oceanic lithosphere age on subduction dynamics (e.g. Molnar and Atwater, 1978; Uyeda and Kanamori, 1979): (1) young oceanic lithosphere is relatively buoyant and resists subduction, causing a gentle slab dip, and high coupling and large compressive stresses at the interface and in the overriding plate, resulting in overriding plate shortening and large earthquakes at the interface; and (2) old oceanic lithosphere has a high negative buoyancy force, sinks steeply into the mantle during slab rollback and causes low coupling and deviatoric tension in the overriding plate and at the subduction zone interface, causing backarc extension and small earthquakes at the interface. Recent work has shown that such conceptual models do not apply to most subduction zones in nature. Subducting plate age does not correlate with backarc deformation style (i.e. shortening, extension, neutral) and backarc deformation rate (Schellart, 2008), nor does it correlate with trench velocity (e.g. Jarrard, 1986; Heuret and Lallemand, 2005; Schellart et al., 2010). These findings suggest that subducting plate age provides no (or only a minor) control on normal stress, mechanical coupling and earthquake magnitude at the subduction zone interface.

The 2004 M_W 9.3 Sumatra–Andaman earthquake violates the age & subduction rate – earthquake size relationship both in terms of subducting plate age (A_{SP} = 57–92 Ma along rupture length) and subduction rate ($v_{S\perp}$ = 1.9–4.6 cm/yr along rupture length). Stein and Okal (2007) revisited the model from Ruff and Kanamori (1980) using an updated dataset and several historical earthquakes, and indeed found that the correlation is much less pronounced. The work did suggest an upper limit for subducting plate age of ~80 Ma for subduction zones that can produce giant earthquakes. The 2011 M_W 9.0 Japan earthquake shows that this upper limit does not apply, as the Pacific plate subducting at the site of this massive earthquake is one of the oldest in the world (~130–134 Ma along rupture length).

A multivariate least-squares linear regression analysis of the dependence of M_W on A_{SP} and $v_{S\perp}$ gives very low correlations, both for the rupture zone dataset (R^2 = 0.05) and for the geological dataset (R^2 = 0.03). This provides further evidence that the combination of plate age and subduction rate is not a good predictor of maximum M_W.

4.4.2. Accretion/erosion rate, and trench and subducted sediment thickness

Ruff (1989) proposed that subduction segments with large sediment thicknesses at the trench and accreting subduction margins promote the occurrence of great earthquakes, arguing that excess trench sediments are associated with the subduction of a coherent sedimentary layer, which forms a homogeneous and strong contact zone at the subduction interface. In such a conceptual model, the homogeneity along the contact zone might allow for a large lateral and down-dip rupture propagation, while the high strength at the contact zone might allow for significant buildup of elastic strain energy and subsequent large coseismic fault slip. It has also been proposed that accreting subduction margins with significant trench sediment fill are generally weak with a low friction coefficient, while subduction margins with small/negligible amounts of trench fill are generally strong and have a high friction coefficient (Lamb and Davis, 2003). The occurrence of giant earthquakes at accreting trenches might then be related to the concept that rupture propagation is facilitated by the low strength of the interface, promoting a large rupture area. The question then remains how such a weak interface will allow for the buildup of significant strain energy to be released in a giant earthquake. Such buildup could potentially occur locally at a high-friction asperity on the interface.

The data in Fig. 3c, k and l, showing the relation between $v_{A\perp}$ and M_W, T_{TS} and M_W and T_{SS} and M_W, provide insight into the possible variability of subduction zone interface strength for subduction zones around the globe. The parameters have low correlations ($|R|$ = 0.03–0.20) and subduction segments with $M_W > 8.5$ have indistinct ranges (70–82%) (Table 2). The data thus indicate that giant earthquakes can occur at accreting subduction margins with large amounts of trench fill and subducted sediments (e.g. southern Chile, Sumatra–Andaman) and eroding subduction segments with small amounts of trench fill and subducted sediments (e.g. Japan, Kamchatka).

If we assume that the conceptual model in which giant earthquakes are facilitated by a mechanically weak subduction zone interface through large rupture propagation is correct, following Lamb and Davis (2003), then this suggests that both accreting subduction margins with thick piles of trench sediments and eroding subduction margins with very small amounts of trench sediments have a comparable (weak) subduction zone interface with a low friction coefficient. If we assume, however, that the conceptual model, in which giant earthquakes with large fault slip are facilitated by a homogeneous mechanically strong subduction zone interface is correct, following Ruff (1989), then this suggests that both types of subduction margins have a comparable (strong) subduction zone interface with a high friction coefficient. Independent of which of the two models applies best to nature, the results suggest that there is not a large variability in subduction interface strength between different subduction zones. Our finding is in agreement with results from von Huene and Ranero (2003), who suggest that along the northern Chile margin (an eroding margin) the subduction interface friction value is comparable to those of

accreting margins. Therefore, the global variability in maximum M_W at subduction zones is related to other parameters.

4.4.3. Convergence velocity

For subduction zones with $M_W > 8.5$, $v_{C\perp} = 0.1–9.5$ cm/yr, which is 79% of the total range (−2.0 to 9.8 cm/yr), indicating that giant earthquakes can occur for very slow to very fast convergence velocities (Fig. 3h).

4.4.4. Lateral slab edge proximity

For subduction zones with $M_W > 8.5$, $D_{SE} = 100–3300$ km, which is 84% of the total range (100–3900 km), indicating that giant earthquakes can occur at trench segments located at distances ranging from very close to very far from the nearest lateral slab edge (Fig. 3s). Heuret et al. (2011) presented a global analysis of subduction zones and subduction zone thrust earthquakes and suggested that subduction zone thrust earthquakes with $M_W \geqslant 8.5$ preferentially occur in the vicinity of lateral slab edges and a neutral overriding plate strain regime (no deformation). The 2011 M_W 9.0 Japan giant earthquake is in disagreement with this conceptual model. The rupture area of the giant earthquake occurred some 2400–2800 km from its closest lateral slab edge in the north (Kamchatka–Aleutians cusp, Fig. 1) in a subduction setting that is classified as highly compressive (Jarrard, 1986; Heuret and Lallemand, 2005) with an overriding plate setting that is characterized by rapid shortening of 2–3 cm/yr (Schellart et al., 2007). A number of giant historical subduction thrust earthquakes have also been reported in the central parts of wide subduction zones (Fig. 1), such as in southern Sumatra (Zachariasen et al., 1999) and in the central Andes (Beck and Ruff, 1989; Dorbath et al., 1990; Chlieh et al., 2011).

In earlier work, Schellart (2008), Schellart et al. (2011) and Schellart and Moresi (2013) proposed a physical mechanism where overriding plate deformation and trench retreat are related to W and D_{SE}, with slow trench migration and overriding plate shortening occurring in the center of wide subduction zones (due to the relative immobility of the subduction zone hinge in the center), and trench retreat and overriding plate extension occurring near lateral slab edges (slab segments near lateral slab edges can roll-back due to efficient toroidal mantle return flow). Such a model can explain the large trench-normal compressive stresses, shortening and low trench velocities in the central Andes and Japan, and might also explain the giant (historic) subduction zone earthquakes observed in these regions. The model can also explain the rapid trench retreat and rapid backarc opening in northern Tonga, southern New Hebrides, southwest Ryukyu and Scotia, and might also explain the absence of any giant earthquakes in these regions ($M_W > 8.5$). However, as stressed in Schellart et al. (2011), although close proximity of a trench segment to a lateral slab edge is a requirement, it does not guarantee rapid trench retreat and back-arc extension, because there are many other circumstances (e.g. subduction of buoyant ridges, plateaus and spreading ridges) that affect $v_{T\perp}$ and $v_{OPD\perp}$. As such, one can also expect giant earthquakes to occur in the vicinity of lateral slab edges, as has indeed been observed, e.g. the 1964 $M_W = 9.2$ Alaska earthquake (Fig. 1).

4.4.5. Deep slab dip, and upper mantle slab length, depth and negative buoyancy

The remaining parameters that show a lack of distinction between observed range for $M_W > 8.5$ and total range include δ_D, L_{UMS}, D_{UMS} and F_{Bu} (75–82%). This indicates that giant earthquakes can occur for subduction segments with gentle to steeply dipping deep slab segments (in the 125–670 km depth range) with a highly variable slab length, depth extent and negative buoyancy force.

5. Conceptual model to explain spatial distribution of giant earthquakes

5.1. Equation for moment magnitude M_W

The moment magnitude M_W is generally calculated as follows (Kanamori, 1986):

$$M_W = (\log E_S - 11.8)/1.5 \quad (1)$$

with

$$E_S = M_0/(2\mu_R/\Delta\sigma) \quad (2)$$

and

$$M_0 = \mu_R DS \quad (3)$$

where E_S is the energy (in ergs) radiated from an earthquake source, μ_R is the rigidity modulus of the material surrounding the fault, $\Delta\sigma$ is the average stress drop in the earthquake, M_0 is the seismic moment, D is the average slip on the fault, and S is the rupture area of the fault plane. If we assume that μ_R is relatively constant for subduction zones around the globe, then the equations indicate that M_W is affected only by D, S and $\Delta\sigma$. From these three parameters, $\Delta\sigma$ is thought to be approximately constant from small earthquakes to giant earthquakes (e.g. Kanamori and Anderson, 1975; Shaw, 2009), although values generally fall within a range that stretches two orders of magnitude (Ruff, 1999). For some giant earthquakes such as the 2011 M_W 9.0 Japan earthquake reported stress drops are relatively large, including 2–10 MPa (Simons et al., 2011) and ~20 MPa (Hasegawa et al., 2011). For the 2010 M_W 8.8 Chile earthquake a depth-averaged stress drop of 4 MPa and a peak static shear stress drop of 17 MPa at the main slip asperity have been reported (Luttrell et al., 2011). Also, for giant earthquakes D is very large, with meters to tens of meters of fault slip. The most important component that makes an earthquake a giant earthquake, however, is fault rupture area (Ruff, 1989). For giant earthquakes the rupture area can be up to a few hundred thousand square km. Below we will discuss how the subduction zone parameters $v_{OPD\perp}$, $v_{T\perp}$, $v_{SP\perp}/v_{S\perp}$, δ_{ST}, C_T, C_{ST}, α_T and $v_{S\perp}$ might affect the magnitude of the parameters D, $\Delta\sigma$, and S.

5.2. Fault slip and stress drop

Coseismic slip on a subduction zone thrust fault plane requires the buildup of (recoverable) elastic strain energy. Such strain energy is (at least partially) released during an earthquake resulting in a stress drop. If the stress drop is not unusually high for a giant earthquake, then its strain is roughly the same as that for small earthquakes but distributed over a larger area. The larger slip in the giant earthquake could then be a consequence of a larger volume storing the strain. It appears, however, that at least for the two most recent giant earthquakes the stress drop is relatively high (see Section 5.1), in particular at the main slip asperity, which is most likely the result of stored high elastic strain. Recent investigations also indicate a near-complete stress drop for the three most recent giant earthquakes (Hardebeck, 2012). High elastic strain energy stored around the subduction zone plate interface can only be sustained by high friction coefficients at the subduction zone interface, or significant compressive normal stress on the fault plane (or a combination thereof) to keep it temporarily locked.

It has been suggested that the amount of sediments in the trench, and the style of accretion at the subduction zone, determines to a large extent the subduction zone friction coefficient, with small amounts of trench sediments and trench erosion causing a high coefficient and large amounts of sediments and trench accretion causing a low coefficient (e.g. Lamb and Davis, 2003). A high friction coefficient is capable of sustaining larger shear stres-

ses at the subduction zone interface than a low friction coefficient, keeping all else equal. Thus it appears plausible that high-friction subduction zone segments can sustain large elastic strains, and can cause a large earthquake with large coseismic slip and a significant stress drop, while those segments with a low friction coefficient cannot. However, as discussed in Section 4.4.2, the data show that for $M_W > 8.5$ subduction segments can be rapidly accreting ($v_{A\perp}$ = 0.3–0.6 cm/yr, e.g. northern Sumatra–Andaman, southern Chile) with significant trench sediments, or rapidly eroding ($v_{A\perp} = -0.3$ cm/yr, e.g. North Japan, Kamchatka) with minor trench sediments (Figs. 3c, 4c). This suggests that friction coefficients at subduction zone thrust faults worldwide are generally comparable for both accreting trench segments and eroding trench segments. This still leaves the question as to whether friction coefficients are generally high or generally low at the subduction zone interface. A low subduction interface strength is implied by investigations of fault rock properties from the subduction zone interface (Moore and Lockner, 2007), regional seismic studies of subduction zones (Magee and Zoback, 1993; Wang et al., 1995; Luttrell et al., 2011), studies of thrust wedge tapers (Suppe, 2007), regional heat flow studies of the subduction zone forearc (Springer, 1999; Grevemeyer et al., 2003) and geodynamic modeling studies of subduction (King and Hager, 1990; Moresi and Solomatov, 1998; Duarte et al., 2013).

From the paragraph above it appears plausible that global variability of the friction coefficient at the subduction zone interface is relatively small and that friction coefficients are generally very low. Thus, the friction coefficient might only play a minor or even a negligible role in determining the global variability in average coseismic slip distance and coseismic stress drop. It might be that the variability in deviatoric normal stress on the subduction zone thrust fault largely determines variability in fault slip and stress drop: Subduction thrust faults with a relatively high normal stress (deviatoric compression with overriding plate shortening, Fig. 5) would promote large elastic strain energy to buildup that can be released in a giant earthquake with a large displacement and a considerable stress drop. Conversely, subduction thrust faults with a relatively low normal stress (deviatoric tension with overriding plate extension, Fig. 5) would promote smaller elastic strain energy to buildup, which can be released in a small earthquake with minor fault slip and a normal stress drop.

A relatively high normal stress state on the subduction interface for subduction segments with $M_W > 8.5$ agrees with the observations for $v_{OPD\perp}$ as no significant trench-normal overriding plate extension/spreading occurs ($v_{OPD\perp} = -3.0$ to 2.2 cm/yr) for subduction segments with $M_W > 8.5$. And notably, $v_{OPD\perp} \leqslant 0$ for subduction segments with epicenters of $M_W > 8.5$ earthquakes (Fig. 3a). For those subduction zones that do have rapid backarc extension/spreading (e.g. Scotia, New Hebrides, Tonga, southern Ryukyu) large earthquakes with $M_W > 8.5$ have not been reported.

The discussion on the requirement of relatively large normal stress on the subduction interface for $M_W > 8.5$ earthquakes does have an apparent caveat. Indeed, it has been proposed that large lateral rupture propagation (which is required for $M_W > 8.5$ earthquakes, see next section) can only occur for a relatively smooth subduction zone interface and a low mechanical coupling (Lamb and Davis, 2003; Heuret et al., 2011), which implies a low friction coefficient and a low normal stress. A potential solution will be provided in Section 5.4 for the three largest recorded earthquakes.

5.3. Rupture area

A large fault rupture area requires a large trench-normal (downdip) extent and trench-parallel extent of the rupture plane. A large trench-normal extent is promoted by a gentle thrust dip angle, because the seismogenic zone where subduction zone interface thrust earthquakes occur has a limited depth range. The downdip extent of the seismogenic zone and the brittle-ductile transition are generally thought to depend on the thermal state of the subduction zone, and the maximum depth for subduction zones around the world is estimated at 30–70 km (Pacheco et al., 1993; Tichelaar and Ruff, 1993; Heuret et al., 2011) with an average of ~50 km. The absolute minimum depth of the seismogenic zone is the depth of the trench, as, for example, was the case for the 2011 M_W 9.0 Japan earthquake (Ide et al., 2011; Kido et al., 2011). So if we assume a seismogenic zone from ~8 km depth (trench depth) down to 50 km depth, then the down-dip extent of the seismogenic zone is 162–242 km for δ_{ST} = 10–15° (e.g. eastern Alaska) but only 53–84 km for δ_{ST} = 30–53° (e.g. New Hebrides). The data for δ_{ST} are all low (10–30°) for $M_W > 8.5$ (Figs. 3m, 4m), implying that a gentle δ_{ST} and a large down-dip extent of the seismogenic zone are indeed required for the generation of giant earthquakes. Note that we did not specifically investigate the seismogenic zone downdip length, as it follows directly from δ_{ST}, the trench depth (which is relatively constant) and our assumption that for all subduction zones the seismogenic zone continues down to 50 km depth.

The trench-parallel extent of the rupture plane is expected to be influenced by many subduction zone parameters. One can intuitively expect a large trench-parallel rupture extent for subduction zones that have a generally straight trench and planar subduction zone thrust interface (i.e. low curvature), because a laterally propagating rupture plane will most likely have more difficulty following a highly concave subduction zone interface such as for Scotia or a convex arc cusp. As such, one can expect low values of C_T, C_{ST} and α_T for $M_W > 8.5$. This is indeed observed (Fig. 3u–w). One can also expect a smooth top surface of the subducting plate entering the trench, because subduction of bathymetrically elevated features such as aseismic ridges, plateaus, seamounts or fracture zones might form barriers to the lateral propagation of a rupture plane (e.g. Ruff, 1989; Lay et al., 1982; Kelleher and McCann, 1976; Contreras-Reyes and Carrizo, 2011). Indeed, the three largest earthquakes in recorded history (Chile 1960, Alaska 1964 and Sumatra–Andaman 2004) with very large lateral rupture propagation (800–1300 km) occurred at subduction segments with very significant trench sediment thicknesses, implying a smooth subduction zone interface. Elevated features, in particular aseismic ridges and fracture zones, might also form nucleation points for giant earthquakes, as recent studies suggest (Contreras-Reyes and Carrizo, 2011; Carena, 2011; Müller and Landgrebe, 2012). Contreras-Reyes and Carrizo (2011) argue that subduction of such features, if elevated, locally increases the normal stress and coupling on the subduction zone interface.

5.4. The largest recorded subduction zone earthquakes

We will now turn our discussion to the largest recorded subduction zone thrust earthquakes. The three largest recorded earthquakes are the 1960 M_W 9.5 Central Chile earthquake, the 1964 M_W 9.2 Alaska earthquake and the 2004 Sumatra–Andaman M_W 9.1–9.3 earthquake, which are characterized by extreme lateral rupture propagation (~1000, ~800 and ~1300 km, respectively). What these earthquakes have in common is that they show unilateral rupture propagation (Figs. 6–8). What these earthquakes further have in common is that the rupture started in a region bordered by an overriding plate segment characterized by active trench-normal shortening and that the rupture propagated unilaterally towards a region bordered by an overriding plate segment with active trench-normal extension or a neutral strain regime. As shown schematically in Fig. 5 using the Mohr–Coulomb failure criterion, a subduction segment bordered by an overriding plate characterized by trench-normal shortening (in the forearc, intra-arc

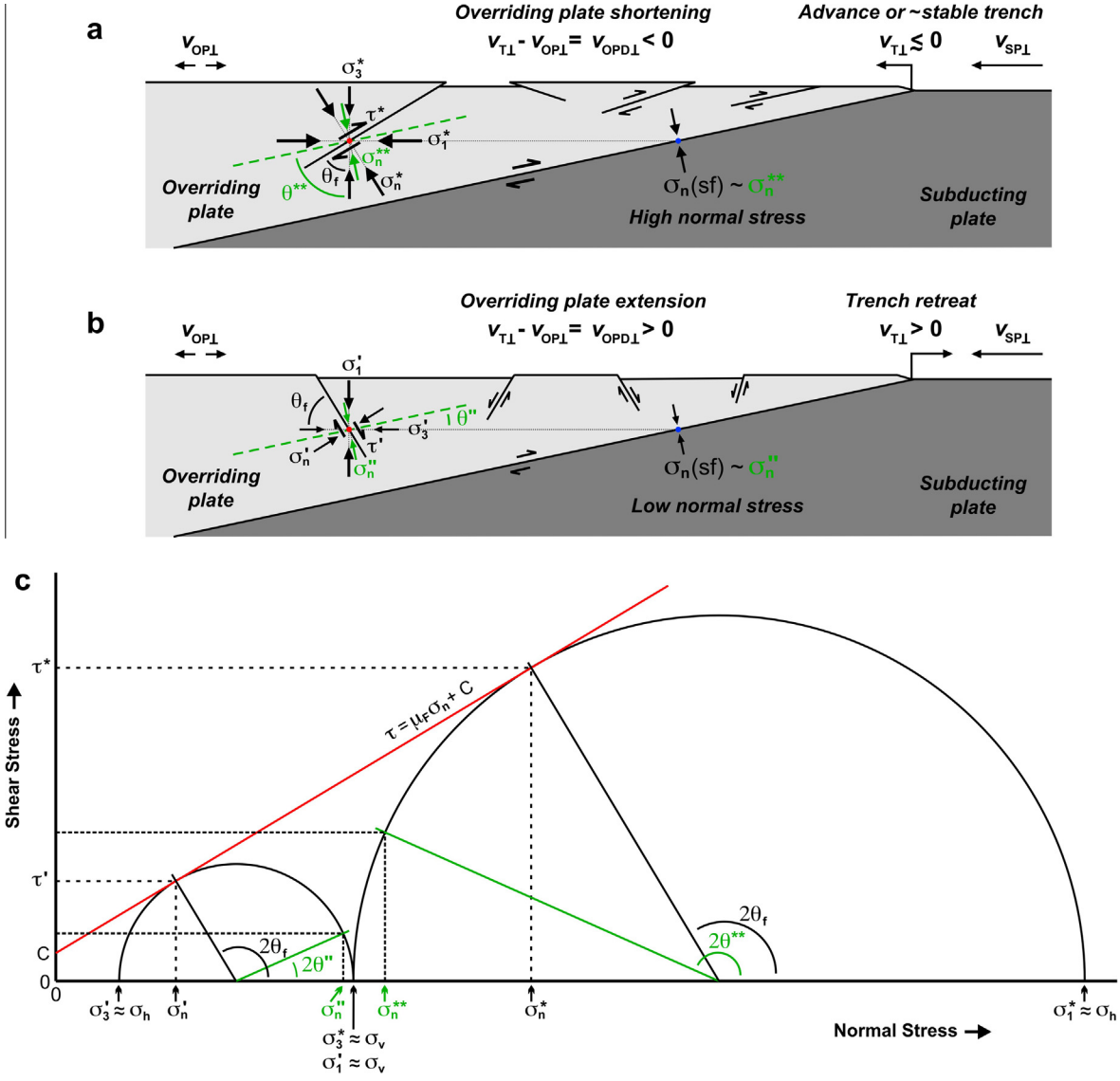

Fig. 5. Schematic cross-sections and diagram illustrating the normal stress on the subduction zone interface (σ_n(sf)) for two different tectonic settings in the overriding plate. (a) Cross-section illustrating overriding plate shortening with the development of thrust faults, implying a relatively high σ_n(sf) (deviatoric compression). $\sigma_1{}^*$ and $\sigma_3{}^*$ are the maximum and minimum principal stress; $\sigma_n{}^*$ and τ^* are the normal stress and shear stress on the thrust fault; $\sigma_n{}^{**}$ is the normal stress on the plane (green dashed line) dipping parallel to the subduction zone fault. (b) Cross-section illustrating overriding plate extension with the development of normal faults, implying a relatively low σ_n(sf) (deviatoric tension). σ_1' and σ_3' are the maximum and minimum principal stress; σ_n' and τ' are the normal stress and shear stress on the normal fault; σ_n'' is the normal stress on the plane (green dashed line) dipping parallel to the subduction zone fault. (c) Normal stress-shear stress diagram showing the Coulomb failure criterion (red line, where τ is the shear stress, μ_F is the coefficient of internal friction, σ_n is the normal stress and C is the cohesion) and two Mohr circles. Large Mohr circle on the right is for the shortening regime in (a) and small Mohr circle on the left is for the extensional regime in (b). Note that σ_h is the maximum horizontal stress, σ_v is the vertical stress, θ_f is the fracture angle, and θ is the angle between the minimum principal stress and the green dashed line in (a, b). (For interpretation of the references to color in this figure legend, the reader is referred to the web version of this article.)

and backarc) experiences relatively high normal stress on the subduction zone interface (deviatoric compression). In contrast, a subduction segment bordered by an overriding plate characterized by trench-normal extension experiences lower normal stress on the subduction zone interface. For an overriding plate that experiences shortening, the maximum deviatoric principal stress $\sigma_1{}^*$ is approximately horizontal, and the minimum deviatoric principal stress $\sigma_3{}^*$ is the vertical stress (σ_v) (Fig. 5a and c). The normal stress on a plane dipping parallel to the subduction fault ($\sigma_n{}^{**}$ in Fig. 5a and c) will be relatively high (deviatoric compression), indicating that the normal stress on the subduction zone fault itself (σ_n(sf) in Fig. 5a) will also be relatively high. For an overriding plate that experiences extension, the maximum deviatoric principal stress $\sigma_1' = \sigma_v$, and the minimum deviatoric principal stress σ_3' is approximately horizontal (Fig. 5b and c). The normal stress (σ_n'') on a plane dipping parallel to the subduction fault will be relatively low (deviatoric tension), indicating that the normal stress (σ_n(sf)) on the subduction zone fault itself will also be relatively low (low deviatoric compression or deviatoric tension) (Fig. 5b and c). In conclusion, for the three largest earthquakes the rupture started in a region of high normal stress on the subduction zone interface and propagated to a zone of lower normal stress on the subduction zone interface.

The high mechanical coupling in the regions of rupture initiation is thus not necessarily because of a local high friction coefficient at the interface, but is (at least partly) because of a high compressive normal stress at the subduction zone interface. With increasing normal stress on the subduction fault an increasingly

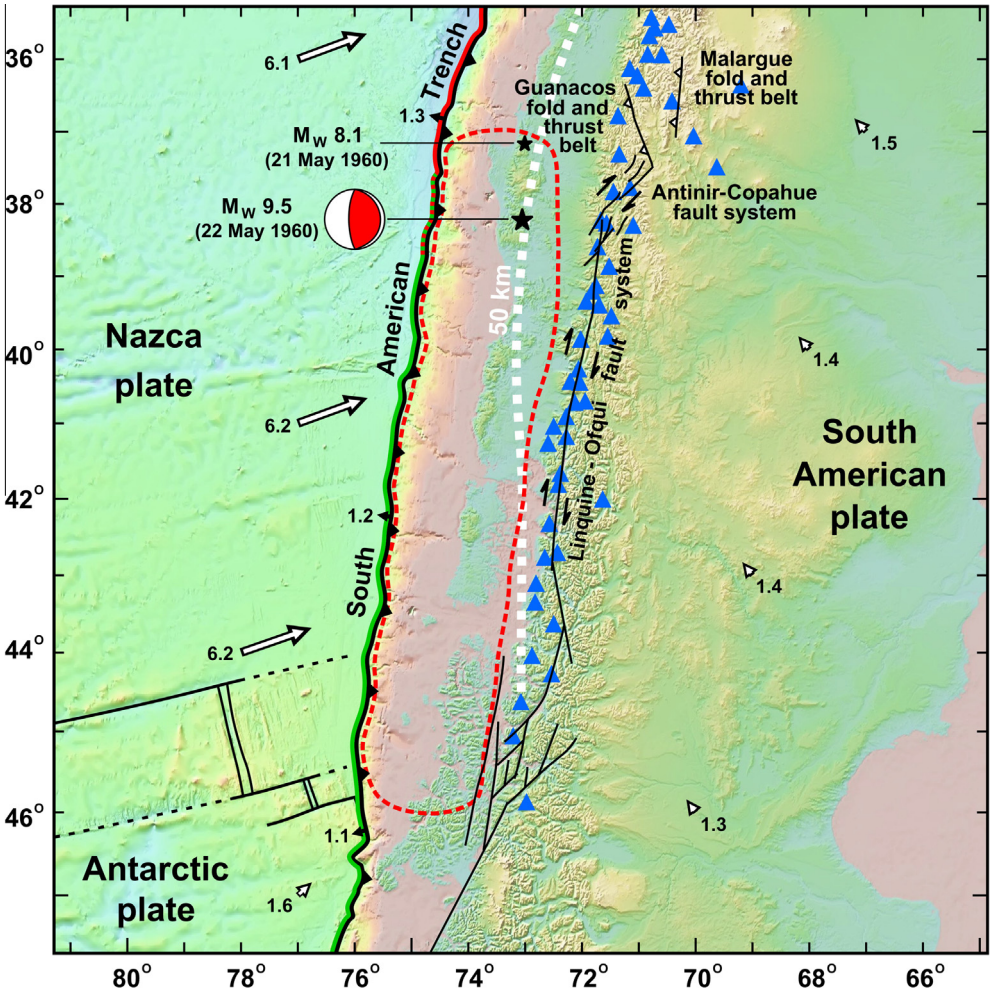

Fig. 6. Tectonic map showing the subduction setting of the 1960 M_W 9.5 Chile earthquake. White arrows with black outline indicate plate velocities, while black arrows at the subduction zone plate boundary indicate trench-normal trench velocities. Numbers indicate velocity in cm/yr. Velocities calculated in the Indo-Atlantic hotspot references frame from O'Neill et al. (2005). White dotted line indicates 50 km depth contour of the top of the slab (from Gudmundsson and Sambridge, 1998). Red dashed line outlines the approximate rupture area of the 1960 M_W 9.5 subduction zone thrust earthquake based on Plafker and Savage (1970) and Moreno et al. (2009). Location of the M_W 8.1 earthquake is from Cifuentes (1989), while focal mechanism and location of the M_W 9.5 earthquake is from Moreno et al. (2009). Structures in the Guanacos fold and thrust belt region are simplified from Folguera et al. (2007). Background bathymetry and topography are from Sandwell and Smith (2009). Colored lines along subduction zone trench indicate active deformation regime in the overriding plate (red – shortening; green – neutral). Blue triangles indicate active volcanoes. (For interpretation of the references to color in this figure legend, the reader is referred to the web version of this article.)

larger shear stress is required to allow slip along a fault plane. Thus, the deviatoric compressive normal stress keeps the subduction zone interface locked for a relatively long time and allows the buildup of high elastic strain energy, which can be released during a giant earthquake with a large fault slip and considerable stress drop, while a large lateral rupture propagation is allowed towards regions with a lower normal stress on the subduction interface. A dominant role of the normal stress, rather than the friction coefficient, has been proposed for determining the seismic coupling coefficient at subduction zones worldwide (Scholz and Campos, 2012).

The data for all the giant earthquakes with $M_W > 8.5$ show that their epicenters all occur at trench segments with $v_{OPD\perp} \leqslant 0$ (Fig. 3a, black diamonds with $M_W > 8.5$), supporting our conceptual model. In the asperity model (e.g. Lay et al., 1982), it is generally thought that an asperity is a local area on the fault plane with a high strength (i.e. high mechanical coupling). At such an asperity, the strength is relatively high compared to the average strength on the fault plane. Such a high strength can be because of a high friction coefficient (high μ_F) on a local part of the fault plane compared to the surrounding region with lower friction coefficients (low μ_F), or because of a local high normal stress on the fault plane compared to the surrounding. For the three greatest earthquakes, and possibly other earthquakes, it appears plausible that the high mechanical coupling at the asperity (i.e. the epicenter zone) is a case of relatively high normal stress on the subduction fault. Thus, variation in mechanical coupling could be explained by variation in normal stress on a subduction fault along which the friction coefficient is relatively constant but with high normal stress at an asperity (which we can call a normal stress asperity), rather than an asperity with a relatively high friction coefficient compared to the surrounding (which we can call a frictional asperity). For the three giant earthquakes a frictional asperity scenario appears less likely than a scenario with a normal stress asperity because these three examples are characterized by sediment-filled trenches and high trench accretion rates along the entire rupture zone length (T_{TS} = ~2–3, ~2 and ~5 km and $v_{A\perp}$ = 0.3, 0.2 and 0.6 cm/yr for Chile, Alaska and Sumatra–Andaman, respectively), suggesting a laterally homogeneous subduction zone interface.

One can also use geodynamic models of subduction and structural geological observations of the overriding plate regions at the hypocenters of the three largest recorded earthquakes

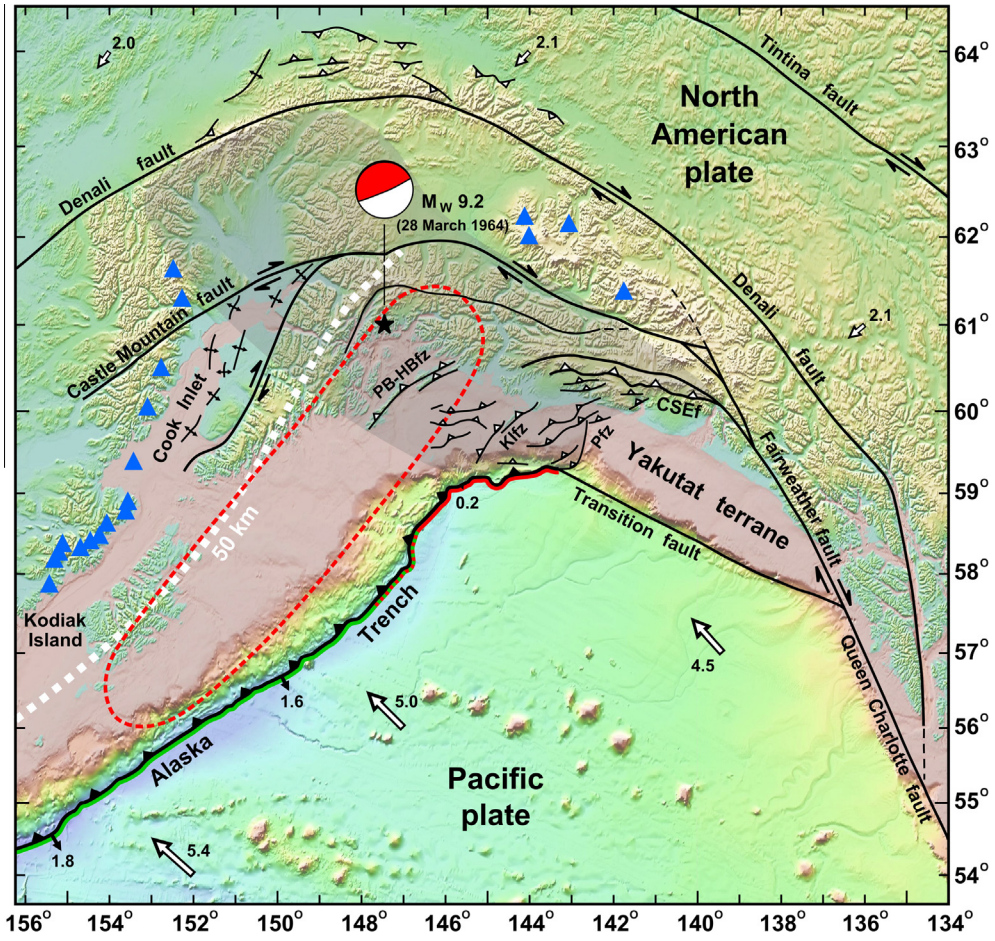

Fig. 7. Tectonic map showing the subduction setting of the 1964 M_W 9.2 Alaska earthquake. Red dashed line outlines the approximate rupture area of the earthquake based on Plafker (1965), Kanamori (1970b) and Christensen and Beck (1994). Epicenter location is from Plafker (1965), while focal mechanism solution is from Christensen and Beck (1994). Thrust structures of the Klfz, Pfz and CSEf are simplified from Bruhn et al. (2004) and Gulick et al. (2007). Fold patterns in the Cook Inlet region are simplified from Bruhn and Haeussler (2006). Fold and thrust structures north of the Denali fault are simplified from Bemis et al. (2012). Grey shaded area indicates extent of Yakutat terrane that has been thrust under Alaska (from Koons et al. (2010) based on data from Eberhart-Phillips et al. (2006)). Background bathymetry and topography are from Sandwell and Smith (2009). Colored lines along subduction zone trench indicate active deformation regime in the overriding plate (red – shortening; green – neutral). For an explanation of other symbols and notation see figure caption of Fig. 6. CSEf – Chugach-St. Elias fault; Klfz – Kayak Island fault zone; PB-HBfz – Patton Bay-Hanning Bay fault zone; Pfz – Pamplona fault zone. (For interpretation of the references to color in this figure legend, the reader is referred to the web version of this article.)

(Figs. 6–8) to distinguish between the possible existence of a frictional asperity or a normal stress asperity at the subduction zone interface. Using geodynamic subduction models, Schellart and Moresi (2013) found that low-medium friction at the subduction zone interface causes horizontal deviatoric compression at a short length scale normal to the trench (forearc region, within ~125 km from the trench), while high compressive deviatoric normal stresses at the subduction zone interface affect the forearc and the backarc region at a length scale up to 500–600 km from the trench. From investigating the spatial extent of deformation in the overriding plate for the three biggest recorded earthquakes (Figs. 6–8) one can observe that at the epicenter location, trench-normal shortening is observed up to ~450 km (Chile), ~400 km (Sumatra) and ~600 km (Alaska) from the trench. The large distances for these three cases therefore suggest that the high deviatoric stress in the overriding plate is the result of a normal stress asperity at the subduction zone interface, not a frictional asperity.

5.4.1. The 1960 M_W 9.5 Chile earthquake

The 1960 M_W 9.5 Chile earthquake occurred at a ~1000 km long subduction segment along a rupture plane that is thought to extend from ~37°S to ~46°S (Fig. 6) (Plafker and Savage, 1970; Cifuentes, 1989; Moreno et al., 2009). The subduction segment is retreating slowly westward ($v_{T\perp}$ = 1.2–1.4 cm/yr) with a mildly compressive overriding plate stress regime with very slow shortening in the northernmost part to a neutral stress regime with regions of no active deformation or possible very slow extension further south. Subduction is dominated by trenchward subducting plate motion ($v_{SP\perp}/v_{S\perp}$ = 0.79–0.83) and moderately high subduction rates ($v_{S\perp}$ = 6.5–6.8 cm/yr), along a very gentle subduction zone thrust (δ_{ST} = 12–16°) with minor trench and thrust curvature ($C_T = 6.9 \times 10^{-17}$–$3.7 \times 10^{-14}$ m^{-2}, $C_{ST} = 1.9 \times 10^{-17}$–$2.0 \times 10^{-14}$ m^{-2}) and small trench curvature angles (α_T = −1.9° to 4.6°). The values of these physical subduction zone parameters show favorable conditions for generating giant earthquakes.

The epicenter of the main earthquake with M_W 9.5 occurred on 22 May 1960 at ~38.0°S and was preceded by an initial M_W 8.1 earthquake that occurred to the north on 21 May 1960 with an epicenter at ~37.2°S (Cifuentes, 1989). The main shock showed southward rupture propagation as far south as the intersection of the Chile spreading ridge with the subduction zone. The tectonic setting in the Andean mountain range in the overriding plate shows there is a major north to south transition at 37–38°S from active Andean shortening and mountain building to absence of shortening (Dewey and Lamb, 1992; Folguera et al., 2004; Folguera et al., 2006a). Structural fieldwork points to shortening and transpressive deformation in the Antinir-Copahue fault system zone down to

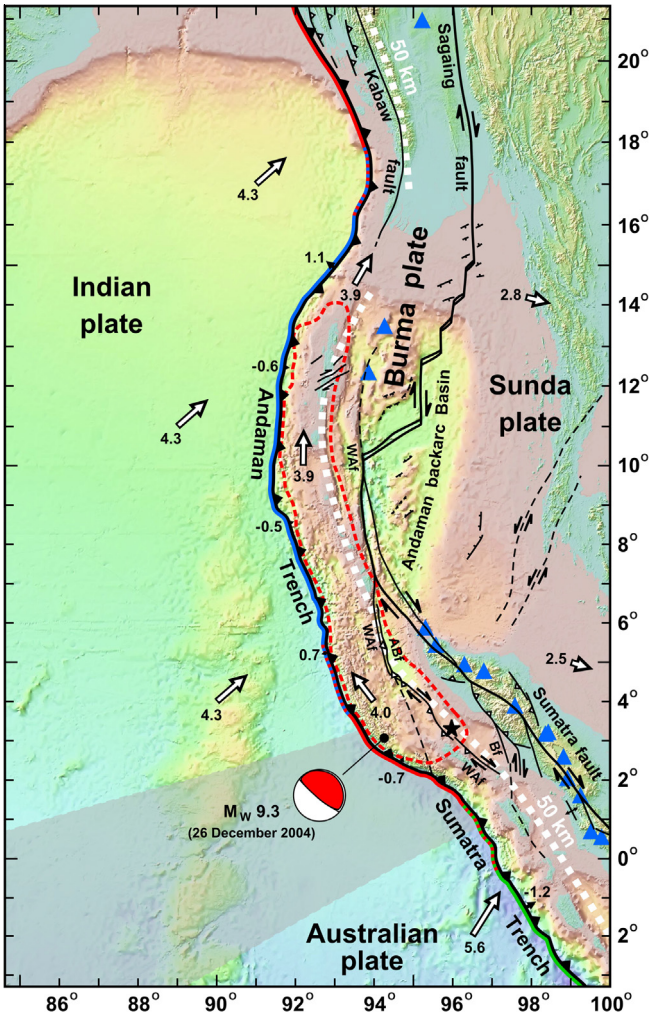

Fig. 8. Tectonic map showing the subduction setting of the 2004 M_W 9.3 Sumatra–Andaman subduction zone thrust earthquake. Red dashed line outlines the approximate rupture area of the M_W 9.3 earthquake based on Ammon et al. (2005) and Shearer and Bürgmann (2010). Epicenter location is from Lay et al. (2005), while moment tensor solution is from the GCMT catalog (note that centroid location is to the west of epicenter). Structures in the Andaman backarc region are simplified from Curray (2005), while ABf is from Singh et al. (2010). Background bathymetry and topography are from Sandwell and Smith (2009). Semi-transparent grey zone in Indian Ocean region indicates diffuse plate boundary between Indian plate and Australian plate. Colored lines along subduction zone trench indicate active deformation regime in the overriding plate (red – shortening; green – neutral; blue – extension). For an explanation of other symbols and notation see figure caption of Fig. 6. ABf – Aceh Basin fault; Bf – Battee fault; =WAf – West Andaman fault. (For interpretation of the references to color in this figure legend, the reader is referred to the web version of this article.)

~38°S in the eastern orogenic front of the main cordillera, but absence of shortening and a neutral overriding plate south of ~38° with locally potential minor extension (Folguera et al., 2004, 2006a,b). The initial and main earthquakes thus occurred in the region of the transition zone in the overriding plate with compression and transpression, implying a deviatoric compressive normal stress on the subduction zone interface, while the rupture propagated southward into a region characterized by a neutral strain regime or possibly minor overriding plate extension, implying lower normal stresses (neutral or minor deviatoric tension) on the interface.

5.4.2. The 1964 M_W 9.2 Alaska earthquake

The 1964 M_W 9.2 Alaska earthquake occurred at an ~800 km long subduction segment (Plafker, 1965) that is retreating slowly southward ($v_{T\perp}$ = 0.2–1.6 cm/yr) with slow overriding plate shortening in the easternmost part and a neutral overriding plate in the west (Fig. 7). Subduction is dominated by trenchward subducting plate motion ($v_{SP\perp}/v_{S\perp}$ = 0.76–0.92) and moderately high subduction rates ($v_{S\perp}$ = 5.0–6.7 cm/yr), along a very gentle subduction zone thrust (δ_{ST} = 10–15°) with minor-moderate trench and thrust curvature ($C_T = 2.2 \times 10^{-15}$–$1.8 \times 10^{-13}$ m^{-2}, $C_{ST} = 5.5 \times 10^{-16}$–$3.8 \times 10^{-14}$ m^{-2}) and small trench curvature angles (α_T = −1.0° to 2.3°).

The epicenter of the 1964 earthquake was at ~61°N ~147.5°W (Plafker, 1965), which is in the Prince William Sound region at the northeastern end of the Aleutian-Alaska subduction zone. The earthquake showed unilateral rupture propagation of ~800 km towards the Kodiak Island region in the southwest. The tectonic setting in both the overriding plate and subducting plate shows considerable variability from northeast to southwest across the region of the rupture zone. In the northeast underthrusting and flat-slab subduction of the Yakutat terrane takes place, while in the southwest normal subduction of Pacific plate oceanic lithosphere occurs (Ferris et al., 2003; Eberhart-Phillips et al., 2006). The boundary between the plateau and the oceanic lithosphere strikes ~NW–SE and the subducted part of this boundary is thought to pass below the easternmost part of the Cook Inlet (Eberhart-Phillips et al., 2006), which is located ~100–130 km to the west of the 1964 earthquake epicenter. The earthquake epicenter is located within a zone of active compressive to transpressive deformation with the Chugach-St Elias thrust zone to the east (Bruhn et al., 2004), forearc shortening and thrusting in the offshore region to the south and southeast including the Pamplona fault zone and Kayak Island fault zone (Carlson and Molnia, 1977; Bruhn et al., 2004; Gulick et al., 2007), reverse faulting in the Patton Bay-Hanning Bay fault zone (Plafker, 1965; Ferguson et al., 2011), strike-slip faulting and folding in the Cook inlet region (Bruhn and Haeussler, 2006) and thrusting north of the Denali fault (Bemis et al., 2012). Active transpressive deformation in the region of the epicenter is evident from upper plate earthquake activity with a combination of thrust-type and strike-slip type earthquake focal mechanisms pointing towards dextral shear of ~0.5 cm/yr in combination with NW-SE oriented (trench-normal) shortening of ~0.3 cm/yr (Leonard et al., 2008). Towards the southwest subduction of normal oceanic lithosphere of the Pacific plate occurs, and the overriding plate here is characterized by a relatively neutral strain regime without significant permanent (non-elastic) deformation as suggested by the low level of overriding plate seismicity on Kodiak Island, the southwest Kenai Peninsula, surrounding offshore regions, and the Alaska Peninsula (Doser et al., 2002). The rupture of the giant 1964 earthquake thus started in a region of overriding plate shortening due to compression and transpression, implying relatively high deviatoric compressive normal stresses on the subduction zone interface, while the rupture propagated southwestward into a region characterized by a neutral overriding plate, implying low deviatoric normal stresses on the subduction zone interface.

5.4.3. The 2004 M_W 9.3 Sumatra–Andaman earthquake

The 2004 M_W 9.3 Sumatra–Andaman earthquake occurred at a ~1300 km subduction segment (Lay et al., 2005; Stein and Okal, 2005; Ni et al., 2005) with an approximately stationary trench ($v_{T\perp}$ = −0.7 to 0.7 cm/yr) with a mildly compressive overriding plate stress regime in the south (with slow overriding plate shortening) changing to a mildly-moderately tensional overriding plate stress regime towards the Andaman islands in the north with an extending overriding plate due to the opening of the Andaman backarc basin east of the Andaman-Nicobar Islands (Fig. 8). Subduction is dominated by trenchward subducting plate motion ($v_{SP\perp}/v_{S\perp}$ = 0.85–1.25) and low subduction rates ($v_{S\perp}$ = 1.9–

4.6 cm/yr), along a gentle subduction zone thrust (δ_{ST} = 12–20°) with minor-moderate trench and thrust curvature (C_T = 1.1 × 10^{-14}–9.4 × 10^{-13} m^{-2}, C_{ST} = 2.9 × 10^{-15}–2.0 × 10^{-13} m^{-2}) and small-intermediate trench curvature angles (α_T = 1.1–9.8°).

The epicenter of the 2004 earthquake is at 3.3°N 96.0°E, which is west of northern Sumatra, and the earthquake showed unilateral northward rupture propagation towards the Nicobar and Andaman Islands as far as 14°N (Lay et al., 2005). The tectonic setting in the overriding plate shows considerable variability from south to north, with a continental overriding plate in the south (north Sumatra segment) and an oceanic overriding plate (actively opening Andaman backarc basin) north of ~6°N (Andaman-Nicobar segment). The north Sumatra segment is characterized by active shortening in the forearc, intra-arc and backarc, as indicated by geological and geophysical studies: Seismic reflection studies of the offshore forearc region show active shortening along southwest-dipping reverse faults (Mosher et al., 2008); Geological studies of the onshore intra-arc zone show active thrust faulting and reverse faulting in the Aceh and Tripa regions of northernmost Sumatra (Sieh and Natawidjaja, 2000); Seismological data show dextral centroid moment tensor solutions for earthquakes along the Sumatra fault in the intra-arc region and reverse/thrust faulting centroid moment tensor solutions for earthquakes in the backarc region (McCaffrey, 2009). In addition, the Euler parameters from Bird (2003) that quantify the relative motion between the Burma plate (BU, located west of the Andaman spreading ridge and the Sumatra fault) and the Sunda plate (SU, to the east) point towards active overriding plate shortening ($v_{OPD\perp} \approx 0.4$ cm/yr) along the trench segment that borders the 2004 earthquake epicenter. The Andaman-Nicobar segment is bordered by the actively opening Andaman backarc basin. This basin is not a standard backarc basin (with most opening occurring in a direction normal to the trench) as it formed mostly by transtension along a complex dextral fault system between the arc "sliver plate" (Burma plate) and the main overriding plate (Sunda plate) (Curray, 2005). The driving mechanism is generally thought to be the highly oblique convergence between the Indian and Sunda plates. Although most of the opening indeed occurs in a direction parallel to the trench, the BU-SU relative plate motion parameters from Bird (2003) indicate that there is also a trench-normal component pointing to trench-normal backarc opening. Calculations indicate that $v_{OPD\perp} \approx$ 1.2–2.3 cm/yr along the Andaman-Nicobar segment. The rupture of the 2004 earthquake thus started in the region of overriding plate shortening due to compression and transpression, implying a deviatoric compressive normal stress on the subduction zone interface (Fig. 5a), while the rupture propagated northward into a region characterized by minor-moderate trench-normal overriding plate extension, implying lower normal stresses (deviatoric tension) on the subduction zone interface (Fig. 5b).

5.4.4. Other giant earthquakes

We will now discuss three more giant subduction zone thrust earthquakes in the light of their tectonic setting and the eight physical parameters ($v_{OPD\perp}$, $v_{T\perp}$, $v_{SP\perp}/v_{S\perp}$, δ_{ST}, C_T, C_{ST}, α_T and $v_{S\perp}$) that provide the strongest constraints on the likelihood of giant earthquakes occurring. These include the 1952 M_W 8.8–9.0 Kamchatka earthquake (Kanamori, 1976; Okal, 1992; Johnson and Satake, 1999), the 2010 M_W 8.8 Chile earthquake (Vigny et al., 2011), and the 2011 M_W 9.0 Japan earthquake (Ide et al., 2011; Ozawa et al., 2011; Simons et al., 2011).

The 1952 M_W 8.8–9.0 Kamchatka earthquake occurred at a ~600 km subduction segment (Johnson and Satake, 1999) that is retreating moderately eastward ($v_{T\perp}$ = 2.3–2.6 cm/yr) with a neutral overriding plate stress regime with no deformation. Subduction is dominated by trenchward subducting plate motion ($v_{SP\perp}/v_{S\perp}$ = 0.72–0.75) and high subduction rates ($v_{S\perp}$ = 9.2–9.5 cm/yr), along a moderately dipping subduction zone thrust (δ_{ST} = 25–30°) with minor trench and thrust curvature (C_T = 1.8 × 10^{-16}–4.4 × 10^{-14} m^{-2}, C_{ST} = 9.1 × 10^{-17}–2.0 × 10^{-14} m^{-2}) and a small trench curvature angle (α_T = 0.2–2.7°).

The 2010 M_W 8.8 Chile (Maule) earthquake occurred at a ~550 km subduction segment (Vigny et al., 2011) that is retreating slowly westward ($v_{T\perp}$ = 1.2–1.4 cm/yr) with a mildly to moderately compressive overriding plate stress regime with no deformation to moderate shortening rates ($v_{OPD\perp} \approx -0.3$ to 0 cm/yr). Subduction is dominated by trenchward subducting plate motion ($v_{SP\perp}/v_{S\perp}$ = 0.76–0.80) and moderately high subduction rates ($v_{S\perp}$ = 5.8–6.7 cm/yr), along a gentle subduction zone thrust (δ_{ST} = 16°) with minor-moderate trench and thrust curvature (C_T = 3.8 × 10^{-14}–1.2 × 10^{-13} m^{-2}, C_{ST} = 2.1 × 10^{-14}–7.0 × 10^{-14} m^{-2}) and a small trench curvature angle (α_T = −3.8° to 2.2°).

The 2011 M_W 9.0 Japan earthquake occurred at a ~400–450 km subduction segment (Ide et al., 2011; Ozawa et al., 2011) that is advancing westward ($v_{T\perp}$ = −2.9 to −2.8 cm/yr) with a highly compressive overriding plate stress regime with fast overriding plate shortening ($v_{OPD\perp}$ = −3.0 to −2.7 cm/yr). Subduction is dominated by trenchward subducting plate motion ($v_{SP\perp}/v_{S\perp}$ = 1.20) and moderately high subduction rates ($v_{S\perp}$ = 6.7 cm/yr), along a gentle subduction zone thrust (δ_{ST} = 16°) with minor-moderate trench and thrust curvature (C_T = 3.6 × 10^{-16}–2.2 × 10^{-13} m^{-2}, C_{ST} = 1.0 × 10^{-16}–6.2 × 10^{-14} m^{-2}) and a small trench curvature angle (α_T = 0.2–5.2°).

A difference between the Chile 2010 and Japan 2011 earthquakes and the largest three reported in Sections 5.4.1, 5.4.2 and 5.4.3 is that the former two show bilateral rupture propagation. The trench-parallel rupture extent was also more limited (~450–550 km). These differences might be (partly) due to the compressive setting at the subduction zone interface along the entire rupture length for both the Chile 2010 and Japan 2011 earthquakes, which would likely have suppressed lateral rupture propagation. This is in contrast to the Chile 1960, Alaska 1964 and Sumatra–Andaman 2004 quakes, for which the epicenter regions characterized by deviatoric compression were flanked on one side by a neutral or deviatoric tensional normal stress regime at the subduction zone interface, promoting lateral rupture propagation towards these regions, but on the other side by a compressive stress regime (i.e. north of ~37°S for Chile, Fig. 6, and east of ~145°W for Alaska, Fig. 7) or a trench cusp (at ~2°N 96°E for Sumatra–Andaman), likely suppressing lateral rupture propagation towards these regions.

6. Predicted spatial distribution for giant earthquakes with $M_W > 8.5$

It has been proposed by McCaffrey (2008) that any subduction zone segment can produce a giant subduction zone thrust earthquake with $M_W \geqslant$ ~9, given enough time (i.e. hundreds to thousands of years). Although the datasets presented here indicate that many physical parameters do not discriminate against earthquake size (e.g. $v_{A\perp}$, $v_{C\perp}$, A_{SP}, D_{SE}, T_{TS}, T_{SS}, δ_D, L_{UMS}, D_{UMS}, F_{Bu}), several parameters appear to do so, most notably $v_{OPD\perp}$, $v_{T\perp}$, δ_{ST}, $v_{SP\perp}/v_{S\perp}$, C_T, C_{ST} and α_T. As such, we argue that there are certain subduction zones and segments that are not capable of producing giant earthquakes. Below we will apply our findings to some of the better-quantified historic giant subduction zone thrust earthquakes, for which the rupture extent and M_W are approximately known. We will investigate if these events fall within the ranges for the discriminating parameters as suggested by our 1900–2012 earthquake dataset. We will also discuss which subduction zone segments are more likely or less likely to produce a giant thrust earthquake in the future in the light of our findings on controlling

Table 4
Ranges for seven subduction zone parameters (200 km datasets) for four historic giant earthquakes (for entire rupture zone extent).

Parameter	Cascadia 1700 M_W ~9	South Sumatra 1833 M_W ~8.8–9.2	South Peru 1868 M_W ~8.8–9.2	North Chile 1877 M_W ~8.8
$v_{OPD\perp}$	−0.4 to 0.6	0	−1.1 to −0.7	−1.5 to −1.3
$v_{T\perp}$ (IA)	1.9–2.7	−0.9 to −0.7	−1.4 to −0.8	−1.0 to −0.4
$v_{SP\perp}/v_{S\perp}$ (IA)	0.3–0.5	1.1–1.2	1.2–1.4	1.1–1.2
δ_{ST}	11–16	14–15	15–18	15–16
C_T	3.1×10^{-14}–2.2×10^{-13}	1.5×10^{-15}–1.4×10^{-13}	2.6×10^{-16}–4.1×10^{-13}	1.5×10^{-14}–1.1×10^{-12}
C_{ST}	7.0×10^{-15}–8.7×10^{-14}	4.0×10^{-16}–3.3×10^{-14}	6.6×10^{-17}–1.1×10^{-13}	3.8×10^{-15}–3.0×10^{-13}
α_T	−7.7 to 5.2	0.4–4.0	−7.2 to 2.3	−11.6 to −1.5

For an explanation of the subduction zone parameters and their units see Table 1. Note that (IA) refers to the Indo-Atlantic moving hotspot reference frame from O'Neill et al. (2005).

subduction zone parameters. Note that the current work does not provide any constraints on when a giant earthquake might take place.

6.1. Historic giant earthquakes

Historic giant subduction earthquakes with $M_W > 8.5$ include the 1700 M_W ~9 Cascadia earthquake (Satake et al., 2003), the 1833 M_W ~8.8–9.2 southern Sumatra earthquake (Zachariasen et al., 1999), and the 1868 M_W ~8.8–9.2 southern Peru and 1877 M_W ~8.8 northern Chile earthquakes just north and south of the Arica bend (Beck and Ruff, 1989; Dorbath et al., 1990; Chlieh et al., 2011; Okal et al., 2006). The lateral rupture extent of these four historic earthquakes is approximately known (see Fig. 1). The values of the subduction zone parameters $v_{OPD\perp}$, $v_{T\perp}$, δ_{ST}, $v_{SP\perp}/v_{S\perp}$, C_{ST} and α_T for the rupture zone segments of these four historic earthquakes are shown in Table 4.

The $v_{OPD\perp}$, $v_{T\perp}$ and δ_{ST} values for the four historic earthquakes all fall within the range for the 1900–2012 subduction thrust earthquakes with $M_W > 8.5$ as presented in Fig. 3 and Table 2. What is more, for the 1833 Sumatra earthquake the other values also fall within the range, as well as those for the 1868 southern Peru quake and the 1700 Cascadia quake, except that they have a slightly lower minimum α_T (−7.2° and −7.7°, respectively) than that for the 1900–2012 $M_W > 8.5$ earthquakes (−6.3°). For the northern Chile 1877 earthquake the maxima for C_T and C_{ST} are slightly higher than those for the 1900–2012 $M_W > 8.5$ earthquakes, while the minimum α_T (−11.6°) is significantly lower than that for the 1900–2012 $M_W > 8.5$ quakes (−6.3°). The trench segment with $\alpha_T = -11.6°$ sits at the northern extent of the 1877 rupture zone and its high curvature might have prevented propagation of the rupture past this zone of high curvature.

6.2. Predicting future locations of giant subduction earthquakes

The compilations presented in Fig. 3 and Table 2 imply that several of the subduction zone parameters provide a control on the spatial occurrence of giant subduction zone thrust earthquakes, including $v_{OPD\perp}$, $v_{T\perp}$, δ_{ST}, $v_{SP\perp}/v_{S\perp}$, C_T, C_{ST} and α_T. The observed ranges of these parameters for segments with $M_W > 8.5$ are relatively narrow (Fig. 3), and the probability that they would result from mere chance is very low ($P = 0.001$–0.003 for RZD, Table 2). The parameters suggest that those subduction segments with rapid backarc opening ($v_{OPD\perp} > \sim 3$ cm/yr), rapid trench retreat ($v_{T\perp} > \sim 3$ cm/yr), a steep subduction thrust ($\delta_{ST} > \sim 30°$), low partitioning ($v_{SP\perp}/v_{S\perp} < 0.3$) or high curvature ($C_T > 1 \times 10^{-12}$ m^{-2}, $C_{ST} > 2 \times 10^{-13}$ m^{-2}, $|\alpha_T| > 10°$) are incapable of producing $M_W > 8.5$ earthquakes. In Fig. 9 we present a global map of the active subduction zones, where the 200 km trench segments have been ranked in terms of their predicted capability of generating a giant subduction zone earthquake with $M_W > 8.5$. A high score means a high predicted capability and vice versa. We have ranked the segments in terms of the six subduction zone parameters that appear to provide a control on the spatial occurrence of giant subduction zone thrust earthquakes ($v_{OPD\perp}$, $v_{T\perp}$, δ_{ST}, $v_{SP\perp}/v_{S\perp}$, C_{ST} and α_T). Note that we have excluded C_T because of the high interdependence of C_T and C_{ST} ($R = 0.94$, see Section 2.1). For the lowest possible score ($S = 0$), the values of the six parameters of a particular trench segment are all outside the range observed for $M_W > 8.5$ earthquakes (using the rupture zone dataset for ranges). For the highest possible score ($S = 6$), the values are all inside the range.

6.3. Subduction segments with high probability of $M_W > 8.5$ earthquakes

In general, the map in Fig. 9 shows a large number of segments with high scores. From a total of 241 subduction zone segments, 222 have been ranked (19 could not be ranked due to a lack of data), and of these 105 segments have the highest score ($S = 6$). This indicates that, on a global scale, at least 44% of the active subduction zone segments posses six out of six important physical characteristics, predicting they are capable of generating giant subduction zone thrust earthquakes with $M_W > 8.5$. Another 42 segments have the second highest score ($S = 5$). The intermediate scores and low scores all have lower numbers, with $n = 35$ for $S = 4$, $n = 17$ for $S = 3$, $n = 14$ for $S = 2$, $n = 8$ for $S = 1$ and $n = 1$ for $S = 0$.

If we look at Fig. 9 in more detail, then the map shows that all subduction segments, for which an $M_W > 8.5$ earthquake has been recorded (a total of 32 segments), have the highest score ($S = 6$), as expected. The map further shows several other subduction zone regions with high scores ($S = 5$, 6). These regions include most of the South American subduction zone, from the Chile Ridge triple junction to northern Bolivia, (average $S = 5.8$, range = 4–6), the entire Aleutians-Alaska subduction zone (average $S = 5.9$, range = 5–6), the entire Sunda subduction zone except for its northernmost segment in northern Andaman (average $S = 5.9$, range = 5–6), the Japan-Kamchatka segment (average $S = 5.2$, range = 4–6), the northern Ryukyu-Nankai segment (average $S = 5.4$, range = 4–6), the entire Cascadia subduction zone (average $S = 5.6$, range = 5–6), most of the Central America-Mexico subduction zone (average $S = 5.8$, range = 4–6), the Makran subduction zone (average $S = 5.8$, range = 5–6), the Lesser Antilles-Puerto Rico subduction zone (average $S = 5.1$, range = 4–6) and the southern Kermadec-Hikurangi subduction segment (average $S = 5.3$, range = 4–6). Several smaller subduction zones also have high scores, including the North Sulawesi subduction zone (average $S = 6$), Manila (three middle segments with $S = 5$) the Calabria subduction zone (average $S = 5.5$, range = 5–6) and central Hellenic (two segments with $S = 5$ and 6).

If we take the conceptual model developed in Section 5.4 for the three largest subduction zone earthquakes and apply it to other subduction zone regions shown in Fig. 9 with high scores, then several regions jump out due to their comparable tectonic setting.

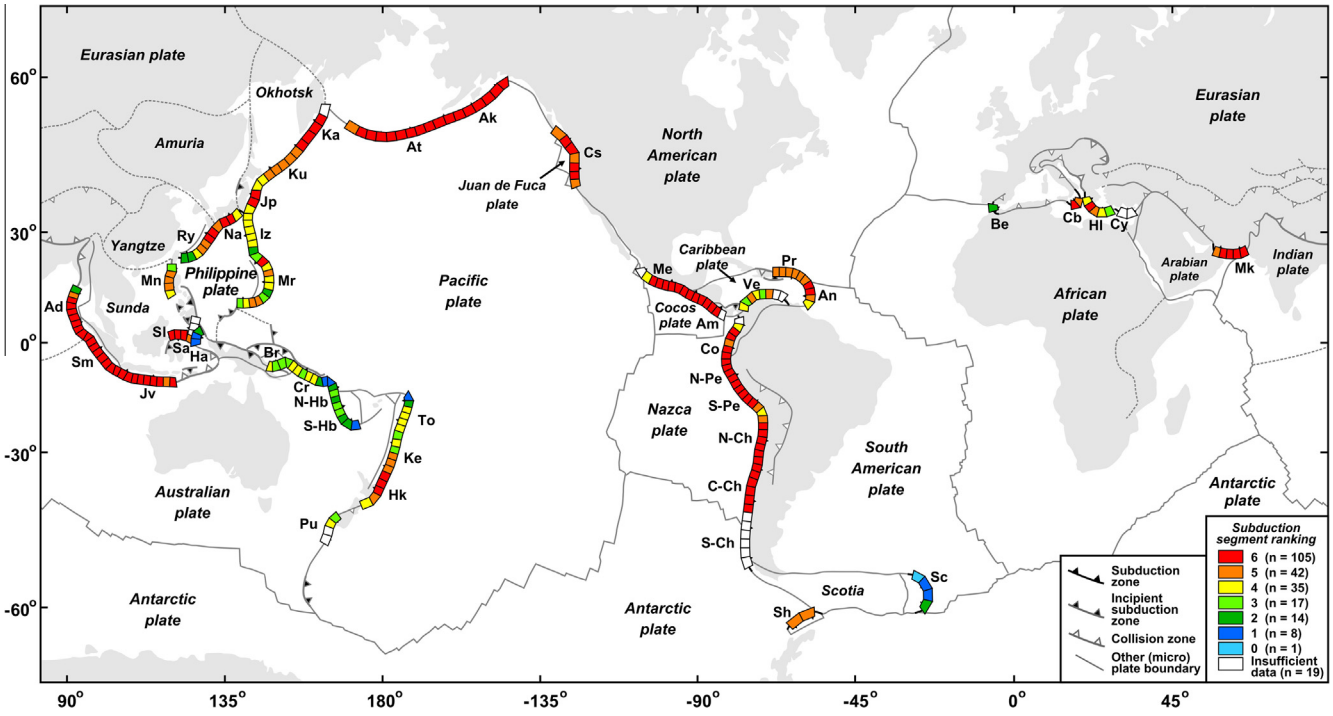

Fig. 9. Global map of the active subduction zones, where the 200 km trench segments have been ranked in terms of their predicted capability of generating a giant subduction zone earthquake with $M_W > 8.5$. The segments have been ranked in terms of six subduction zone parameters: trench-normal overriding plate deformation rate ($v_{OPD\perp}$), trench-normal trench velocity ($v_{T\perp}$), subduction thrust dip angle (δ_{ST}), subduction partitioning ($v_{SP\perp}/v_{S\perp}$), subduction thrust curvature (C_{ST}) and trench curvature angle (α_T). For the lowest possible score ($S = 0$), the values of the six parameters of a particular trench segment are all outside the ranges observed for $M_W > 8.5$ earthquakes (using the rupture zone dataset for ranges, see Fig. 3 and Table 2), implying a low risk of producing an $M_W > 8.5$ earthquake. For the highest possible score ($S = 6$), all six values are inside the ranges, implying a high risk of producing an $M_W > 8.5$ earthquake. Abbreviations for the subduction zone segments are explained in the figure caption of Fig. 1.

These regions include the Hikurangi-southern Kermadec subduction segment and the Central America subduction segment. Other regions could include the Nankai-northeastern Ryukyu subduction segment, the western Hellenic subduction segment, the Lesser Antilles-Puerto Rico subduction zone and the Manila subduction zone. Below we will describe the Hikurangi-southern Kermadec subduction segment and the Central America subduction segment in more detail.

6.3.1. The Hikurangi-southern Kermadec subduction zone segment

The Hikurangi-southern Kermadec subduction segment forms the southern part of the Tonga-Kermadec-Hikurangi subduction zone with west-northwestward subduction of the Pacific plate below the Australian plate (Fig. 10). The Kermadec trench and northernmost Hikurangi trench are flanked by the Kermadec arc and the Havre Trough, an active backarc basin with extension at 1–2 cm/yr in the south (Wright, 1993; Bird, 2003; Power et al., 2012). The central Hikurangi margin is flanked by the Axial Ranges and the Taupo volcanic zone to the west, the latter of which is an active continental backarc basin with active extension at ~1.5 cm/yr in the north and decreasing southward to <0.5 cm/yr at 39°S (Wallace et al., 2004). Further to the south, the southernmost Hikurangi margin is characterized by overriding plate shortening west of the Axial Ranges with active northwest-southeast shortening in the Kapiti–Manawatu fault system of the southeastern Wanganui Basin (Lamarche et al., 2005; Barnes et al., 2010). Geodetic investigations predict an oblique shortening rate of 0.1–0.4 cm/yr here (Wallace et al., 2004).

The trench-parallel gradient in overriding plate deformation implies relatively high normal stress (deviatoric compression) on the subduction zone interface in the southwest changing to relatively low normal stress (deviatoric tension) towards the northeast (Fig. 10). In analogy with the tectonic settings of the Chile 1960, Alaska 1964 and Sumatra–Andaman 2004 giant earthquakes, one could expect a giant subduction earthquake with an epicenter at the subduction zone plate interface in the southwest Hikurangi region, and unilateral rupture propagation towards the northeast. Fig. 9 shows relatively high scores ($S = 4$–5) for the two southernmost Hikurangi segments, and the highest scores for the next three segments to the north ($S = 6$). Wallace et al. (2009) documented high interseismic coupling coefficients (0.8–1.0) in the south but lower ones (0.1–0.2) in the central and northern Hikurangi region, suggesting higher elastic strain buildup in the south.

6.3.2. The Central America subduction zone segment

The Central America subduction segment forms part of the Mexico-Central America subduction zone with northeastward subduction of the Cocos plate below the North American plate in the northwest, the Caribbean plate in the middle and the Panama plate in the southeast (Fig. 11). In the southeast the buoyant Cocos Ridge indents and subducts below the Panama plate, causing active overriding plate shortening in the inner forearc (Fila Costena thrust belt) and outer forearc (e.g. Burica Peninsula) as indicated by structural investigations (Fisher et al., 2004; Sitchler et al., 2007; Morell et al., 2011) and geodetic investigations (LaFemina et al., 2009). It also causes backarc shortening where thrusting is observed at the Panama-Caribbean plate boundary (Silver et al., 1990), and at the northern boundary of the inactive arc and in the Limon backarc region north of the inactive arc (Morell et al., 2012). Towards the northwest there is structural, geological, geomorphological and geochemical evidence for active slow extension (~0.3–0.6 cm/yr) in the intra-arc region in Nicaragua (Phipps Morgan et al., 2008).

The overriding plate deformation implies relatively high normal stress (deviatoric compression) on the subduction zone interface in the southeast changing to relatively low normal stress (deviatoric tension) towards the northwest. In analogy with the tectonic

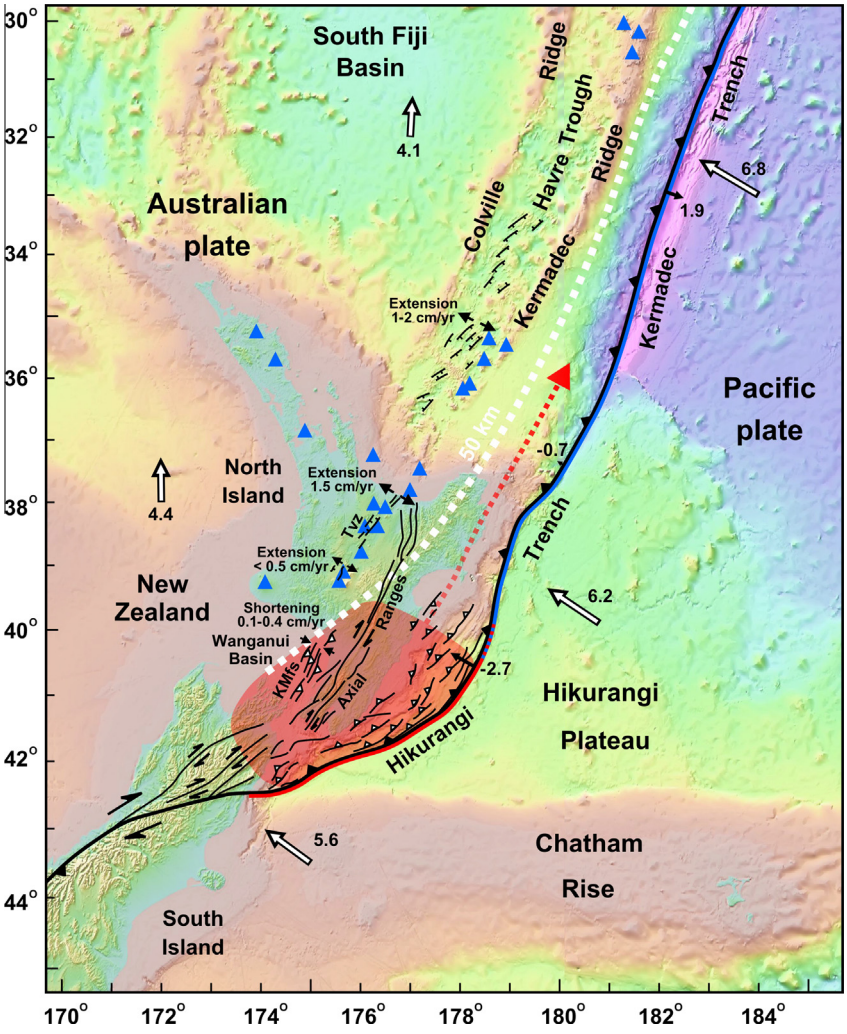

Fig. 10. Tectonic map showing the setting of the Hikurangi-southern Kermadec subduction segment. White arrows with black outline indicate plate velocities, while black arrows at the subduction zone plate boundary indicate trench-normal trench migration velocities. Numbers indicate velocity in cm/yr. Velocities calculated in the Indo-Atlantic hotspot references frame from O'Neill et al. (2005) using the geodetic relative plate motion model from Kreemer et al. (2003). White dotted line indicates 50 km depth contour of the top of the slab (from Gudmundsson and Sambridge, 1998). Background bathymetry and topography are from Sandwell and Smith (2009). Semi-transparent red area indicates predicted region within which the epicenter of a giant earthquake will occur, while red dotted arrow indicates predicted rupture propagation direction. Fault patterns on and immediately off-shore North Island are simplified from Barnes et al. (2010). Colored lines along subduction zone trench indicate active deformation regime in the overriding plate (red – shortening; blue – extension). Blue triangles indicate active volcanoes. KMfs – Kapiti–Manawatu fault system, Tvz – Taupo volcanic zone. (For interpretation of the references to color in this figure legend, the reader is referred to the web version of this article.)

settings of the Chile 1960, Alaska 1964 and Sumatra–Andaman 2004 giant earthquakes, one could expect a giant earthquake with an epicenter in southeast Costa Rica where the Cocos Ridge subducts (deviatoric compression), and unilateral rupture propagation towards the Nicaragua subduction segment in the northwest with low or tensional deviatoric normal stresses on the interface.

6.4. Subduction segments with low probability of $M_W > 8.5$ earthquakes

The map predicts that the Scotia subduction zone is the least likely of all subduction zones to produce $M_W > 8.5$ subduction zone thrust earthquakes (average $S = 1$, observed range = 0–2) due to its rapid backarc opening, rapid trench retreat, steep thrust dip, low partitioning and high curvature (Fig. 9). The map further shows that the New Britain-San Cristobal-New Hebrides subduction zone has low to moderate scores (1–4). In particular, it suggests that the New Hebrides subduction segment is unlikely to produce $M_W > 8.5$ earthquakes (average $S = 2.1$, observed range = 1–3) due to its rapid backarc opening, rapid trench retreat, steep thrust dip, and low partitioning. The Tonga subduction segment is unlikely to produce $M_W > 8.5$ thrust earthquakes mainly due to its very rapid backarc opening and rapid trench retreat (average $S = 3.2$, range = 1–4). The Mariana subduction segment, with moderate scores (average $S = 4.0$, range = 2–6), is also unlikely to produce $M_W > 8.5$ thrust earthquakes, even though it does have one trench segment with a ranking of $S = 6$ and three with a ranking of $S = 5$. These high values are for two isolated trench segments and two adjoining segments that are surrounded by segments with lower values, and thus large lateral rupture propagation is unlikely. Finally, the small Halmahera subduction zone has low scores (average $S = 1.3$, range = 1–2) and is also unlikely to produce $M_W > 8.5$ earthquakes due to its rapid trench retreat, steep slab dip and high curvature.

7. Conclusions

In this paper we have presented global subduction zone datasets for the maximum recorded subduction zone thrust earthquakes that have occurred at active subduction zones around the globe in the period January 1900–June 2012. The datasets illustrate

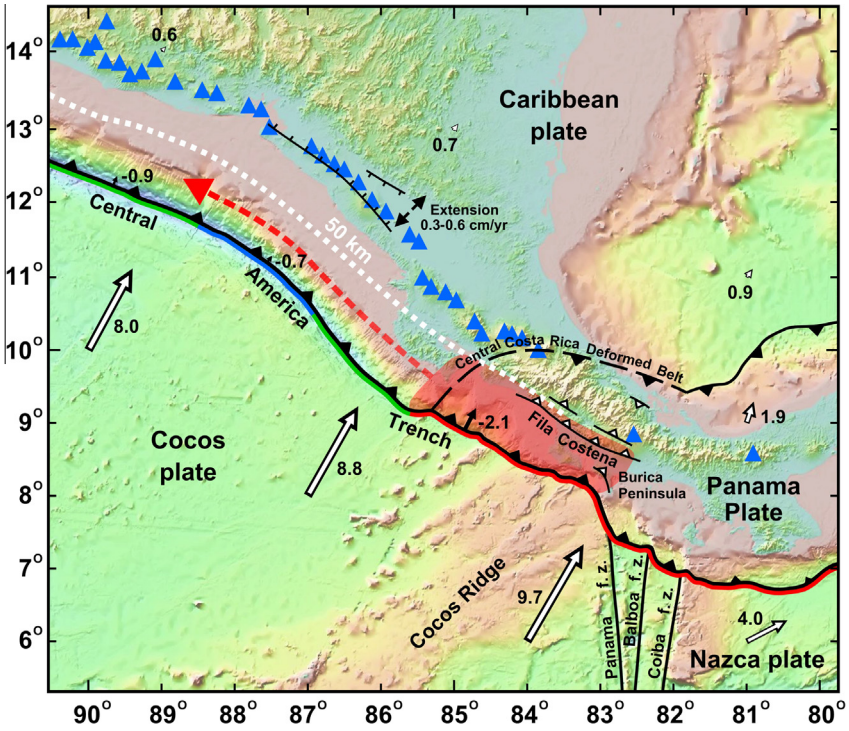

Fig. 11. Tectonic map showing the setting of the Central America subduction segment. Fault pattern in the Fila Costena is simplified from Fisher et al. (2004), while the extensional fault pattern is simplified from Phipps Morgan et al. (2008). Background bathymetry and topography are from Sandwell and Smith (2009). Semi-transparent red area indicates predicted region within which the epicenter of a giant earthquake will occur, while red dashed arrow indicates predicted rupture propagation direction. Colored lines along subduction zone trench indicate active deformation regime in the overriding plate (red – shortening; green – neutral; blue – extension). For an explanation of other symbols and notation see figure caption of Fig. 10. (For interpretation of the references to color in this figure legend, the reader is referred to the web version of this article.)

how the observed spatial variability in M_W might depend on 24 different subduction zone parameters. We draw the following main conclusions from our work:

1. For our (preferred) two datasets, the rupture zone dataset and epicenter dataset (segmentation into 200 km trench segments, maximum of 216 segments with sufficient data), all least-squares linear regression correlations are negligible-low ($|R| = 0.00–0.30$) and statistically insignificant (Fig. 3). The dataset with geologically defined subduction zone segments (maximum of 37 segments with sufficient data) shows negligible-moderate correlations ($|R| = 0.02–0.51$) with the highest correlation for slab width (Fig. 4); only slab width shows a statistically significant correlation at 95% confidence level.
2. For a number of parameters, including slab age, trench accretion/erosion rate, trench sediment thickness and upper mantle slab negative buoyancy force, the low correlations are likely due to the absence of any physical relation between the parameters and earthquake potential of the subduction segments.
3. For several parameters, including overriding plate deformation rate, trench velocity, subduction partitioning, subduction thrust dip angle, subduction thrust curvature and trench curvature angle, the low correlations possibly result from the short period of global instrumental observations, which can be an order of magnitude shorter than the longest recurrence interval of giant subduction zone earthquakes. Indeed, a comparative investigation of the observed ranges of the physical parameters for subduction segments with $M_W > 8.5$ and the observed ranges for all subduction segments show distributions of data points that are not random but are distinct for the above mentioned parameters (Fig. 3) with distinct (narrow) ranges for segments with $M_W > 8.5$.
4. The distinct (narrow) ranges for segments with $M_W > 8.5$ give low values for $v_{OPD\perp}$ (i.e. shortening or relatively neutral overriding plate) and $v_{T\perp}$ (trench advance or slow trench retreat), and high values for $v_{SP\perp}/v_{S\perp}$ (subduction dominated by trenchward subducting plate motion) (Fig. 3). Such values promote relatively high deviatoric normal stresses on the subduction zone interface (deviatoric compression) (Fig. 5a and c), promoting the buildup of high elastic strain energy that can be released in a giant earthquake with a high fault slip (meters to tens of meters) with stress drops of MPa to tens of MPa. High values for $v_{OPD\perp}$ and $v_{T\perp}$ (i.e. rapid extension and trench retreat), and low values for $v_{SP\perp}/v_{S\perp}$ (i.e. subduction dominated by trench retreat), promote relatively low deviatoric normal stresses on the subduction zone interface (i.e. deviatoric tension or neutral stress) (Fig. 5b and c), promoting the buildup of only minor elastic strain energy.
5. The distinct (narrow) ranges for segments with $M_W > 8.5$ give low values for δ_{ST}, C_{ST} and α_T (Fig. 3). Such values promote large rupture propagation parallel to the dip of the subduction zone thrust interface (δ_{ST}) and laterally along the trench (C_{ST} and α_T), thus favoring a large earthquake rupture area (of the order $\sim 10^5$ km^2), which is characteristic of giant earthquakes. Strongly curved subduction zones (either concave or convex) and steep subduction thrust dips likely limit the lateral propagation of the earthquake rupture, while steep dips also limit the downdip extent of the rupture plane.

6. Our research has shown that epicenters of giant earthquakes with $M_W > 8.5$ only occur at trench segments with $v_{OPD\perp} \leqslant 0$ (epicenter dataset in Fig. 3a with black diamonds and green circles), suggesting that such earthquakes initiate at locked segments of the subduction zone interface that have a relatively high normal stress (deviatoric compression) on the subduction zone interface (i.e. a normal stress asperity). Note that the normal stress asperities should be seen separately from asperities that result from variation in friction coefficient along the subduction zone interface (i.e. a frictional asperity). It is evident from the Mohr–Coulomb failure criterion that with increasing normal stress an increase in shear stress is required to allow slip along the subduction zone thrust interface (Fig. 5). The deviatoric normal stress on the subduction interface results from the relative motion between the subduction zone hinge and the overriding plate, with convergence between the two inducing deviatoric compression and divergence causing deviatoric tension. It follows that the spatial probability of the occurrence of giant subduction thrust earthquakes is therefore linked to the large-scale dynamics of the subducting plate, overriding plate, slab and ambient mantle. This is because slab rollback/roll-forward processes and subduction-induced mantle flow patterns provide significant control on the relative motions of the subduction zone hinge and overriding plate (Schellart and Moresi, 2013), and also play an important role in determining trench curvature and slab curvature (Schellart et al., 2007). Another feature of major importance is the presence of buoyant features on the subducting plate, such as plateaus, which affect the local dip angle of the slab, and which can cause local overriding plate shortening and compression at the subduction zone interface, thereby forming a potential nucleation zone for epicenters of giant earthquakes.
7. The current work does not provide any insight into the temporal probability of giant subduction zone thrust earthquakes, but it does give insight into their spatial probability. A number of trench segments of active subduction zones have parametric values for $v_{OPD\perp}$, $v_{T\perp}$, $v_{SP\perp}/v_{S\perp}$, δ_{ST}, C_{ST} and α_T that are in the same range as those trench segments that have experienced $M_W > 8.5$ earthquakes (Fig. 9). These include several subduction segments for which historical giant earthquakes ($M_W > 8.5$) have been reported, in particular Cascadia 1700, southern Sumatra 1833, northern Chile 1877 and southern Peru 1868. There are also segments, including Hikurangi-southern Kermadec and Central America (Figs. 10 and 11), that have comparable tectonic settings to those segments that have experienced the three largest recorded earthquakes (Chile 1960, Alaska 1964 and Sumatra–Andaman 2004, Figs. 6–8), which are characterized by unilateral rupture propagation along the subduction zone interface from a region of compressive normal stress towards a region of neutral stress or deviatoric tension. If the conceptual model as derived from the largest three earthquakes also applies to these regions, then we predict that they will experience a giant subduction zone thrust earthquake in the future.

Acknowledgments

We thank two anonymous reviewers and the editor George Helffrich for their constructive and thoughtful comments. This research was supported by Future Fellowship FT110100560 and Discovery grants DP110103387 and DP120102983 from the Australian Research Council awarded to WPS.

References

Abe, K., 1972. Mechanism and tectonic implications of the 1966 and 1970 Peru earthquakes. Physics of the Earth and Planetary Interiors 5, 367–379.
Agnew, D., Berger, J., Buland, R., Farrell, W., Gilbert, F., 1976. International deployment of accelerometers: a network for very long period seismology. EOS, Transactions American Geophysical Union 57, 180–188. http://dx.doi.org/10.1029/EO057i004p00180.
Allen, T.I., Marano, K., Earle, P.S., Wald, D.J., 2009. PAGER-CAT: a composite earthquake catalog for calibrating global fatality models. Seismological Research Letters 80, 50–56.
Ammon, C.J., Ji, C., Thio, H.-K., Robinson, D., Ni, S., Hjorleifsdottir, V., Kanamori, H., Lay, T., Das, S., Helmberger, D., Ichinose, G., Polet, J., Wald, D., 2005. Rupture process of the 2004 Sumatra–Andaman Earthquake. Science 308, 1133–1139. http://dx.doi.org/10.1126/science.1112260.
Ando, M., 1975. Source mechanisms and tectonic significance of historical earthquakes along the Nankai Trough, Japan. Tectonophysics 27, 119–140.
Barnes, P.M., Lamarche, G., Bialas, J., Henrys, S., Pecher, I., Netzeband, G.L., Greinert, J., Mountjoy, J.J., Pedley, K., Crutchley, G., 2010. Tectonic and geological framework for gas hydrates and cold seeps on the Hikurangi subduction margin, New Zealand. Marine Geology 272, 26–48. http://dx.doi.org/10.1016/j.margeo.2009.03.012.
Beavan, J., Wang, X., Holden, C., Wilson, K., Power, W., Prasetya, G., Bevis, M., Kautoke, R., 2010. Near-simultaneous great earthquakes at Tongan megathrust and outer rise in September 2009. Nature 466, 959–963. http://dx.doi.org/10.1038/nature09292.
Beck, S.L., Christensen, D.H., 1991. Rupture process of the February 4, 1965, Rat Island earthquake. Journal of Geophysical Research 96, 2205–2221.
Beck, S.L., Ruff, L.J., 1987. Rupture process of the great 1963 kurile islands earthquake sequence: asperity interaction and multiple event rupture. Journal of Geophysical Research 92, 14123–14138.
Beck, S.L., Ruff, L.J., 1989. Great earthquakes and subduction along the Peru trench. Physics of the Earth and Planetary Interiors 57, 199–224.
Bemis, S.P., Carver, G.A., Koehler, R.D., 2012. The Quaternary thrust system of the northern Alaska range. Geosphere 8, 196–205. http://dx.doi.org/10.1130/GES00695.1.
Bird, P., 2003. An updated digital model of plate boundaries. Geochemistry Geophysics Geosystems 4, 1027. http://dx.doi.org/10.1029/2001GC000252.
Bruhn, R.L., Haeussler, P.J., 2006. Deformation driven by subduction and microplate collision: geodynamics of Cook Inlet basin, Alaska. Geological Society of America Bulletin 118, 289–303. http://dx.doi.org/10.1130/B25672.1.
Bruhn, R.L., Pavlis, T.L., Plafker, G., Serpa, L., 2004. Deformation during terrane accretion in the Saint Elias orogen, Alaska. Geological Society of America Bulletin 116, 771–787. http://dx.doi.org/10.1130/B25182.1.
Butler, R., Lay, T., Creager, K., Earl, P., Fischer, K., Gaherty, J., Laske, G., Leith, B., Park, J., Ritzwoller, M., Tromp, J., Wen, L., 2004. The global seismographic network surpasses its design goal. EOS, Transactions American Geophysical Union 85, 225–232. http://dx.doi.org/10.1029/2004EO230001.
Byrne, D.E., Sykes, L.R., Davis, D.M., 1992. Great thrust earthquakes and aseismic slip along the plate boundary of the Makran subduction zone. Journal of Geophysical Research 97, 449–478.
Carena, S., 2011. Subducting-plate topography and nucleation of great and giant earthquakes along the South American trench. Seismological Research Letters 82, 629–637.
Carlson, P.R., Molnia, B.F., 1977. Submarine faults and slides on the continental shelf, northern gulf of Alaska. Marine Geotechnology 2, 275–290.
Chlieh, M., Perfettini, H., Tavera, H., Avouac, J.-P., Remy, D., Nocquet, J.-M., Rolandone, F., Bondoux, F., Gabalda, G., Bonvalot, S., 2011. Interseismic coupling and seismic potential along the Central Andes subduction zone. Journal of Geophysical Research 116, B12405. http://dx.doi.org/10.1029/2010JB008166.
Christensen, D.H., Beck, S.L., 1994. The rupture process and tectonic implications of the great 1964 Prince William Sound earthquake. Pure and Applied Geophysics 142, 29–53.
Cifuentes, I.L., 1989. The 1960 Chilean earthquakes. Journal of Geophysical Research 94, 665–680.
Clift, P., Vannucchi, P., 2004. Controls on tectonic accretion versus erosion in subduction zones: implications for the origin and recycling of the continental crust. Reviews of Geophysics 42. http://dx.doi.org/10.1029/2003RG000127, RG2001.
Conrad, C.P., Behn, M.D., 2010. Constraints on lithosphere net rotation and asthenospheric viscosity from global mantle flow models and seismic anisotropy. Geochemistry Geophysics Geosystems 11. http://dx.doi.org/10.1029/2009GC002970, Q05W05.
Conrad, C.P., Bilek, S., Lithgow-Bertelloni, C., 2004. Great earthquakes and slab pull: interaction between seismic coupling and plate-slab coupling. Earth and Planetary Science Letters 218, 109–122.
Contreras-Reyes, E., Carrizo, D., 2011. Control of high oceanic features and subduction channel on earthquake ruptures along the Chile–Peru subduction zone. Physics of the Earth and Planetary Interiors 186, 49–58. http://dx.doi.org/10.1016/j.pepi.2011.03.002.
Curray, J.R., 2005. Tectonics and history of the Andaman Sea region. Journal of Asian Earth Sciences 25, 187–232.
Davies, G.F., Richards, M.A., 1992. Mantle convection. Journal of Geology 100, 151–206.

De Franco, R., Govers, R., Wortel, R., 2008. Nature of the plate contact and subduction zones diversity. Earth and Planetary Science Letters 271, 245–253. http://dx.doi.org/10.1016/j.epsl.2008.04.019.
Dewey, J., Byerly, P., 1969. The early history of seismometry (to 1900). Bulletin of the Seismological Society of America 59, 183–228.
Dewey, J.F., Lamb, S.H., 1992. Active tectonics of the Andes. Tectonophysics 205, 79–95.
Dorbath, L., Cisternas, A., Dorbath, C., 1990. Assessment of the size of large and great historical earthquakes in Peru. Bulletin of the Seismological Society of America 80, 551–576.
Doser, D.I., Brown, W.A., Velasquez, M., 2002. Seismicity of the Kodiak Island region (1964–2001) and its relation to the 1964 great Alaska earthquake. Bulletin of the Seismological Society of America 92, 3269–3292.
Duarte, J.C., Schellart, W.P., Cruden, A.R., 2013. Three-dimensional dynamic laboratory models of subduction with an overriding plate and variable interplate rheology. Geophysical Journal International 195, 47–66. http://dx.doi.org/10.1093/gji/ggt257.
Eberhart-Phillips, D., Christensen, D.H., Brocher, T.M., Hansen, R., Ruppert, N.A., Haeussler, P.J., Abers, G.A., 2006. Imaging the transition from Aleutian subduction to Yakutat collision in central Alaska, with local earthquakes and active source data. Journal of Geophysical Research 111, B11303. http://dx.doi.org/10.1029/2005JB004240.
Elsasser, W.M., 1971. Sea-floor spreading as thermal convection. Journal of Geophysical Research 76, 1101–1112.
Engdahl, E.R., Villaseñor, A., 2002. Global Seismicity: 1900-1999. International handbook of earthquake and engineering seismology, 81A, 665–690.
Ferguson, K., Armstrong, P.A., Haeussler, P.J., Arkle, J.C., 2011. Rock Uplift above the Yakutat Megathrust on Montague Island, Prince William Sound, Alaska. American Geophysical Union Fall Meeting, San Francisco, pp. T33A–2384.
Ferris, A., Abers, G.A., Christensen, D.H., Veenstra, E., 2003. High resolution image of the subducted Pacific (?) plate beneath central Alaska, 50–150 km depth. Earth and Planetary Science Letters 214, 575–588. http://dx.doi.org/10.1016/S0012-821X(03)00403-5.
Fisher, D.M., Gardner, T.W., Sak, P.B., Sanchez, J.D., Murphy, K., Vannucchi, P., 2004. Active thrusting in the inner forearc of an erosive convergent margin, Pacific coast, Costa Rica. Tectonics 23, TC2007. http://dx.doi.org/10.1029/2002TC001464.
Folguera, A., Ramos, V.A., Hermanns, R.L., 2004. Neotectonics in the foothills of the southernmost central Andes (37°_–38_°S): evidence of strike-slip displacement along the Antiñir-Copahue fault zone. Tectonics 23, TC5008. http://dx.doi.org/10.1029/2003TC001533.
Folguera, A., Ramos, V.A., González Díaz, E.F., Hermanns, R., 2006a. Miocene to Quaternary deformation of the Guañacos fold-and-thrust belt in the Neuquén Andes between 37°S and 37°30′S. Geological Society of America Special Paper 407, 247–266. http://dx.doi.org/10.1130/2006.2407(11).
Folguera, A., Zapata, T., Ramos, V.A., 2006b. Late Cenozoic extension and the evolution of the Neuquén Andes. Geological Society of America Special Paper 407, 267–285. http://dx.doi.org/10.1130/2006.2407(12).
Folguera, A., Ramos, V.A., Zapata, T., Spagnuolo, M.G., 2007. Andean evolution at the Guanacos and Chos Malal fold and thrust belts (36°30′_–37°s). Journal of Geodynamics 44, 129–148. http://dx.doi.org/10.1016/j.jog.2007.02.003.
Forsyth, D.W., Uyeda, S., 1975. On the relative importance of the driving forces of plate motion. The Geophysical Journal of the Royal Astronomical Society 43, 163–200.
Grevemeyer, I., Diaz-Naveas, J.L., Ranero, C.R., Villinger, H.W.Ocean Drilling Program Leg 202 Scientific Party, 2003. Heat flow over the descending Nazca plate in central Chile, 32S to 41S: observations from ODP Leg 202 and the occurrence of natural gas hydrates. Earth and Planetary Science Letters 213, 285–298. http://dx.doi.org/10.1016/S0012-821X(03)00303-0.
Gripp, A.E., Gordon, R.G., 2002. Young tracks of hotspots and current plate velocities. Geophysical Journal International 150, 321–361.
Gudmundsson, O., Sambridge, M.J., 1998. A regionalized upper mantle (RUM) seismic model. Journal of Geophysical Research 103, 7121–7136.
Gulick, S.P.S., Lowe, L.A., Pavlis, T.L., Gardner, J.V., Mayer, L.A., 2007. Geophysical insights into the Transition fault debate: propagating strike slip in response to stalling Yakutat block subduction in the Gulf of Alaska. Geology 35, 763–766. http://dx.doi.org/10.1130/G23585A.1.
Hager, B.H., 1984. Subducted slabs and the geoid: constraints on mantle rheology and flow. Journal of Geophysical Research 89, 6003–6015.
Hardebeck, J.L., 2012. Coseismic and postseismic stress rotations due to great subduction zone earthquakes. Geophysical Research Letters 39, L21313. http://dx.doi.org/10.1029/2012GL053438.
Hasegawa, A., Yoshida, K., Okada, T., 2011. Nearly complete stress drop in the 2011 M_W 9.0 off the Pacific coast of Tohoku Earthquake. Earth Planets Space 63, 703–707. http://dx.doi.org/10.5047/eps.2011.06.007.
Heuret, A., Lallemand, S., 2005. Plate motions, slab dynamics and back-arc deformation. Physics of the Earth and Planetary Interiors 149, 31–51.
Heuret, A., Lallemand, S., Funiciello, F., Piromallo, C., Faccenna, C., 2011. Physical characteristics of subduction interface type seismogenic zones revisited. Geochemistry Geophysics Geosystems 12, Q01004. http://dx.doi.org/10.1029/2010GC003230.
Ide, S., Baltay, A., Beroza, G.C., 2011. Shallow dynamic overshoot and energetic deep rupture in the 2011 M_W 9.0 Tohoku-Oki Earthquake. Science 332, 1426–1429. http://dx.doi.org/10.1126/science.1207020.
Jarrard, R.D., 1986. Relations among subduction parameters. Reviews of Geophysics 24, 217–284.
Johnson, J.M., Satake, K., 1999. Asperity distribution of the 1952 great Kamchatka earthquake and its relation to future earthquake potential in Kamchatka. Pure and Applied Geophysics 154, 541–553.
Johnson, J.M., Tanioka, Y., Ruff, L.J., Satake, K., Kanamori, H., Sykes, L.R., 1994. The 1957 great Aleutian earthquake. Pure and Applied Geophysics 142, 3–28.
Kanamori, H., 1970a. Synthesis of long-period surface waves and its application to earthquake source studies-Kuril Islands earthquake of October 13, 1963. Journal of Geophysical Research 75, 5011–5027.
Kanamori, H., 1970b. The Alaska earthquake of 1964: radiation of long-period surface waves and source mechanism. Journal of Geophysical Research 75, 5029–5040.
Kanamori, H., 1972. Tectonic implications of the 1944 Tonankai and the 1946 Nankaido earthquakes. Physics of the Earth and Planetary Interiors 5, 129–139.
Kanamori, H., 1976. Re-examination of the Earth's free oxcillations excited by the Kamchatka earthquake of November 4, 1952. Physics of the Earth and Planetary Interiors 11, 216–226.
Kanamori, H., 1977. The energy release in great earthquakes. Journal of Geophysical Research 82, 2981–2987.
Kanamori, H., 1986. Rupture process of subduction-zone earthquakes. Annual Review Earth and Planetary Sciences 14, 293–322.
Kanamori, H., Anderson, D.L., 1975. Theoretical basis of some empirical relations in seismology. Bulletin of the Seismological Society of America 65, 1073–1095.
Karig, D.E., Caldwell, J.G., Parmentier, E.M., 1976. Effects of accretion on the geometry of the descending lithosphere. Journal of Geophysical Research 81, 6281–6291.
Kelleher, J., McCann, W., 1976. Buoyant zones, great earthquakes, and unstable boundaries of subduction. Journal of Geophysical Research 81, 4885–4896.
Kelleher, J., Savino, J., Rowlett, H., McCann, W., 1974. Why and where great thrust earthquakes occur along island arcs. Journal of Geophysical Research 79, 4889–4899.
Kido, M., Osada, Y., Fujimoto, H., Hino, R., Ito, Y., 2011. Trench-normal variation in observed seafloor displacements associated with the 2011 Tohoku-Oki earthquake. Geophysical Research Letters 38, L24303. http://dx.doi.org/10.1029/2011GL050057.
King, S.D., Hager, B.H., 1990. The relationship between plate velocity and trench viscosity in Newtonian and power-law subduction calculations. Geophysical Research Letters 17, 2409–2412.
Koons, P.O., Hooks, B.P., Pavlis, T., Upton, P., Barker, A.D., 2010. Three-dimensional mechanics of Yakutat convergence in the southern Alaskan plate corner. Tectonics 29, TC4008. http://dx.doi.org/10.1029/2009TC002463.
Kreemer, C., 2009. Absolute plate motions constrained by shear wave splitting orientations with implications for hot spot motions and mantle flow. Journal of Geophysical Research 114, B10405. http://dx.doi.org/10.1029/2009JB006416.
Kreemer, C., Holt, W.E., Haines, A.J., 2003. An integrated global model of present-day plate motions and plate boundary deformation. Geophysical Journal International 154, 8–34.
LaFemina, P., Dixon, T.H., Govers, R., Norabuena, E., Turner, H., Saballos, A., Mattioli, G., Protti, M., Strauch, W., 2009. Fore-arc motion and Cocos Ridge collision in Central America. Geochemistry Geophysics Geosystems 10, Q05S14. http://dx.doi.org/10.1029/2008GC002181.
Lamarche, G., Proust, J.-N., Nodder, S.D., 2005. Long-term slip rates and fault interactions under low contractional strain, Wanganui Basin, New Zealand. Tectonics 24, TC4004. http://dx.doi.org/10.1029/2004TC001699.
Lamb, S., Davis, P., 2003. Cenozoic climate change as a possible cause for the rise of the Andes. Nature 425, 792–797.
Lay, T., Kanamori, H., Ruff, L., 1982. The asperity model and the nature of large subduction zone earthquakes. Earthquake Prediction Research 1, 3–71.
Lay, T., Kanamori, H., Ammon, C.J., Nettles, M., Ward, S.N., Aster, R.C., Beck, S.L., Bilek, S.L., Brudzinski, M.R., Butler, R., DeShon, H.R., Ekstrom, G., Satake, K., Sipkin, S., 2005. The Great Sumatra–Andaman Earthquake of 26 December 2004. Science 308, 1127–1133. http://dx.doi.org/10.1126/science.1112250.
Lay, T., Kanamori, H., Ammon, C.J., Hutko, A.R., Furlong, K., Rivera, L., 2009. The 2006–2007 Kuril Islands great earthquake sequence. Journal of Geophysical Research 114, B11308. http://dx.doi.org/10.1029/2008JB006280.
Lay, T., Ammon, C.J., Kanamori, H., Rivera, L., Koper, K.D., Hutko, A.R., 2010. The 2009 Samoa–Tonga great earthquake triggered doublet. Nature 466, 964–968. http://dx.doi.org/10.1038/nature09214.
Leonard, L.J., Mazzotti, S., Hyndman, R.D., 2008. Deformation rates estimated from earthquakes in the northern Cordillera of Canada and eastern Alaska. Journal of Geophysical Research 113, B08406. http://dx.doi.org/10.1029/2007JB005456.
Llenos, A.L., McGuire, J.J., 2007. Influence of fore-arc structure on the extent of great subduction zone earthquakes. Journal of Geophysical Research 112, B09301. http://dx.doi.org/10.1029/2007JB004944.
López, A.M., Okal, E.A., 2006. A seismological reassessment of the source of the 1946 Aleutian 'tsunami' earthquake. Geophysical Journal International 165, 835–849. http://dx.doi.org/10.1111/j.1365-246X.2006.02899.x.
Luttrell, K.M., Tong, X., Sandwell, D.T., Brooks, B.A., Bevis, M.G., 2011. Estimates of stress drop and crustal tectonic stress from the 27 February 2010 Maule, Chile, earthquake: implications for fault strength. Journal of Geophysical Research 116, B11401. http://dx.doi.org/10.1029/2011JB008509.
Magee, M.E., Zoback, M.D., 1993. Evidence for a weak interplate thrust fault along the northern Japan subduction zone and implications for the mechanics of thrust faulting and fluid expulsion. Geology 21, 809–812.
Matsubara, M., Yagi, Y., Obara, K., 2005. Plate boundary slip associated with the 2003 Off-Tokachi earthquake based on small repeating earthquake data.

Geophysical Research Letters 32, L08316. http://dx.doi.org/10.1029/2004GL022310.
McCaffrey, R., 1993. On the role of the upper plate in great subduction zone earthquakes. Journal of Geophysical Research 98, 11953–11966.
McCaffrey, R., 1997. Influence of recurrence times and fault zone temperatures on the age-rate dependence of subuction zone seismicity. Journal of Geophysical Research 102, 22839–22854.
McCaffrey, R., 2008. Global frequency of magnitude 9 earthquakes. Geology 36, 263–266. http://dx.doi.org/10.1130/G24402A.
McCaffrey, R., 2009. The tectonic framework of the Sumatran subduction zone. Annual Review Earth and Planetary Sciences 37, 345–366. http://dx.doi.org/10.1146/annurev.earth.031208.100212.
McKenzie, D., Jackson, J., Priestley, K., 2005. Thermal structure of oceanic and continental lithosphere. Earth and Planetary Science Letters 233, 337–349.
Minoura, K., Imamura, F., Sugawa, D., Kono, Y., Iwashita, T., 2001. The 869 Jogan tsunami deposit and recurrence interval of large-scale tsunami on the Pacific coast of Northeast Japan. Journal of Natural Disaster Science 23, 83–88.
Molnar, P., Atwater, T., 1978. Interarc spreading and Cordilleran tectonics as alternates related to the age of subducted oceanic lithosphere. Earth and Planetary Science Letters 41, 330–340.
Moore, D.E., Lockner, D.A., 2007. Comparative deformation behavior of minerals in serpentinized ultramafic rock: application to the slab-mantle interface in subduction zones. International Geology Reviews 49, 401–415. http://dx.doi.org/10.2747/0020-6814.49.5.401.
Morell, K.D., Fisher, D.M., Gardner, T.W., La Femina, P., Davidson, D., Teletzke, A., 2011. Quaternary outer fore-arc deformation and uplift inboard of the Panama Triple Junction, Burica Peninsula. Geochemistry Geophysics Geosystems 116, B05402. http://dx.doi.org/10.1029/2010JB007979.
Morell, K.D., Kirby, E., Fisher, D.M., van Soest, M., 2012. Geomorphic and exhumational response of the Central American Volcanic Arc to Cocos Ridge subduction. Journal of Geophysical Research 117, B04409. http://dx.doi.org/10.1029/2011JB008969.
Moreno, M.S., Bolte, J., Klotz, J., Melnick, D., 2009. Impact of megathrust geometry on inversion of coseismic slip from geodetic data: application to the 1960 Chile earthquake. Geophysical Research Letters 36, L16310. http://dx.doi.org/10.1029/2009GL039276.
Moresi, L., Solomatov, V., 1998. Mantle convection with a brittle lithosphere; thoughts on the global tectonic styles of the Earth and Venus. Geophysical Journal International 133, 669–682.
Mosher, D.C., Austin Jr., J.A., Fisher, D., Gulick, S.P.S., 2008. Deformation of the northern Sumatra accretionary prism from high-resolution seismic reflection profiles and ROV observations. Marine Geology 252, 89–99. http://dx.doi.org/10.1016/j.margeo.2008.03.014.
Müller, R.D., Landgrebe, T.C.W., 2012. The link between great earthquakes and the subduction of oceanic fracture zones. Solid Earth 3, 447–465. http://dx.doi.org/10.5194/se-3-447-2012.
Ni, S., Kanamori, H., Helmberger, D., 2005. Energy radiation from the Sumatra earthquake. Nature 434, 582.
Okal, E.A., 1992. Use of the mantle magnitude Mm for the reassessment of the moment of historical earthquakes – I: shallow events. Pure and Applied Geophysics 139, 17–57.
Okal, E.A., Borrero, J.C., Synolakis, C.E., 2006. Evaluation of tsunami risk from regional earthquakes at Pisco, Peru. Bulletin of the Seismological Society of America 96, 1634–1648. http://dx.doi.org/10.1785/0120050158.
Oliver, J., Murphy, L., 1971. WWNSS: seismology's global network of observing stations. Science 174, 254–261.
O'Neill, C., Müller, D., Steinberger, B., 2005. On the uncertainties in hot spot reconstructions and the significance of moving hot spot reference frames. Geochemistry Geophysics Geosystems 6, Q04003. http://dx.doi.org/10.1029/2004GC000784.
Ozawa, S., Nishimura, T., Suito, H., Kobayashi, T., Tobita, M., Imakiire, T., 2011. Coseismic and postseismic slip of the 2011 magnitude-9 Tohoku-Oki earthquake. Nature 475, 373–376. http://dx.doi.org/10.1038/nature10227.
Pacheco, J.F., Sykes, L.R., 1992. Seismic moment catalogue of large shallow earthquakes, 1900 to 1989. Bulletin of the Seismological Society of America 82, 1306–1349.
Pacheco, J.F., Sykes, L.R., Scholz, C.H., 1993. Nature of seismic coupling along simple plate boundaries of the subduction type. Journal of Geophysical Research 98, 14133–14159.
Peterson, E.T., Seno, T., 1984. Factors affecting seismic moment release rates in subduction zones. Journal of Geophysical Research 89, 10233–10248.
Phipps Morgan, J., Ranero, C.R., Vannucchi, P., 2008. Intra-arc extension in Central America: links between plate motions, tectonics, volcanism, and geochemistry. Earth and Planetary Science Letters 272, 365–371. http://dx.doi.org/10.1016/j.epsl.2008.05.004.
Plafker, G., 1965. Tectonic deformation associated with the 1964 Alaska earthquake. Science 148, 1675–1687.
Plafker, G., Savage, J.C., 1970. Mechanism of the Chilean earthquakes of May 21 and 22, 1960. Geological Society of America Bulletin 81, 1001–1030.
Power, W., Wallace, L., Wang, X., Reyners, M., 2012. Tsunami hazard posed to New Zealand by the Kermadec and southern New Hebrides subduction margins: an assessment based on plate boundary kinematics, interseismic coupling, and historical seismicity. Pure and Applied Geophysics 169, 1–36. http://dx.doi.org/10.1007/s00024-011-0299-x.
Ruff, L.J., 1989. Do trench sediments affect great earthquake occurrence in subduction zones? Pure and Applied Geophysics 129, 263–282.
Ruff, L.J., 1999. Dynamic stress drop of recent earthquakes: variations within subduction zones. Pure and Applied Geophysics 154, 409–431.
Ruff, L., Kanamori, H., 1980. Seismicity and the subduction process. Physics of the Earth and Planetary Interiors 23, 240–252.
Sandwell, D.T., Smith, W.H.F., 2009. Global marine gravity from retracked Geosat and ERS-1 altimetry: ridge segmentation versus spreading rate. Journal of Geophysical Research 114, B01411. http://dx.doi.org/10.1029/2008JB006008.
Satake, K., Atwater, B.F., 2007. Long-term perspectives on giant earthquakes and tsunamis at subduction zones. Annual Review Earth and Planetary Sciences 35, 349–374. http://dx.doi.org/10.1146/annurev.earth.35.031306.140302.
Satake, K., Wang, K., Atwater, B.F., 2003. Fault slip and seismic moment of the 1700 Cascadia earthquake inferred from Japanese tsunami descriptions. Journal of Geophysical Research 108, 2535. http://dx.doi.org/10.1029/2003JB002521.
Schellart, W.P., 2008. Overriding plate shortening and extension above subduction zones: a parametric study to explain formation of the Andes mountains. Geological Society of America Bulletin 120, 1441–1454. http://dx.doi.org/10.1130/B26360.1.
Schellart, W.P., 2011. A subduction zone reference frame based on slab geometry and subduction partitioning of plate motion and trench migration. Geophysical Research Letters 38, L16317. http://dx.doi.org/10.1029/2011GL048197.
Schellart, W.P., Moresi, L., 2013. A new driving mechanism for backarc extension and backarc shortening through slab sinking induced toroidal and poloidal mantle flow: results from dynamic subduction models with an overriding plate. Journal of Geophysical Research: Solid Earth 118, 3221–3248. http://dx.doi.org/10.1002/jgrb.50173.
Schellart, W.P., Spakman, W., 2012. Mantle constraints on the plate tectonic evolution of the Tonga-Kermadec-Hikurangi subduction zone and the South Fiji Basin. Australian Journal of Earth Sciences 59, 933–952. http://dx.doi.org/10.1080/08120099.2012.679692.
Schellart, W.P., Freeman, J., Stegman, D.R., Moresi, L., May, D., 2007. Evolution and diversity of subduction zones controlled by slab width. Nature 446, 308–311. http://dx.doi.org/10.1038/nature05615.
Schellart, W.P., Stegman, D.R., Freeman, J., 2008. Global trench migration velocities and slab migration induced upper mantle volume fluxes: constraints to find an Earth reference frame based on minimizing viscous dissipation. Earth-Science Reviews 88, 118–144. http://dx.doi.org/10.1016/j.earscirev.2008.01.005.
Schellart, W.P., Stegman, D.R., Farrington, R.J., Freeman, J., Moresi, L., 2010. Cenozoic tectonics of western North America controlled by evolving width of Farallon slab. Science 329, 316–319. http://dx.doi.org/10.1126/science.1190366.
Schellart, W.P., Stegman, D.R., Farrington, R.J., Moresi, L., 2011. Influence of lateral slab edge distance on plate velocity, trench velocity and subduction partitioning. Journal of Geophysical Research 116, B10408. http://dx.doi.org/10.1029/2011JB008535.
Scholz, C.H., Campos, J., 1995. On the mechanism of seismic decoupling and back arc spreading at subduction zones. Journal of Geophysical Research 100, 22103–22115.
Scholz, C.H., Campos, J., 2012. The seismic coupling of subduction zones revisited. Journal of Geophysical Research 117, B05310. http://dx.doi.org/10.1029/2011JB009003.
Shaw, B.E., 2009. Constant stress drop from small to great earthquakes in magnitude-area scaling. Bulletin of the Seismological Society of America 99, 871–875. http://dx.doi.org/10.1785/0120080006.
Shearer, P., Bürgmann, R., 2010. Lessons learned from the 2004 Sumatra–Andaman megathrust rupture. Annual Review Earth and Planetary Sciences 38, 103–131. http://dx.doi.org/10.1146/annurev-earth-040809-152537.
Sieh, K., Natawidjaja, D., 2000. Neotectonics of the Sumatran fault, Indonesia. Journal of Geophysical Research 105, 28295–28326.
Silver, E.A., Reed, D.L., Tagudin, J.E., Heil, D.J., 1990. Implications of the north and south Panama thrust belts for the origin of the Panama orocline. Tectonics 9, 261–281.
Simons, M., Minson, S.E., Sladen, A., Ortega, F., Jiang, J., Owen, S.E., Meng, L., Ampuero, J.-P., Wei, S., Chu, R., Helmberger, D.V., Kanamori, H., Hetland, E., Moore, A.W., Webb, F.H., 2011. The 2011 Magnitude 9.0 Tohoku-Oki Earthquake: mosaicking the Megathrust from Seconds to Centuries. Science 332, 1421–1425.
Singh, S.C., Hananto, N.D., Chauhan, A.P.S., Permana, H., Denolle, M., Hendriyana, A., Natawidjaja, D., 2010. Evidence of active backthrusting at the NE Margin of Mentawai Islands, SW Sumatra. Geophysical Journal International 180, 703–714. http://dx.doi.org/10.1111/j.1365-246X.2009.04458.x.
Sitchler, J.C., Fisher, D.M., Gardner, T.W., Protti, M., 2007. Constraints on inner forearc deformation from balanced cross sections, Fila Costeña thrust belt, Costa Rica. Tectonics 26, TC6012. http://dx.doi.org/10.1029/2006TC001949.
Springer, M., 1999. Interpretation of heat-flow density in the Central Andes. Tectonophysics 306, 377–395.
Stauder, W., 1968. Mechanism of the Rat Island earthquake sequence of February 4, 1965, with relation to island arcs and sea-floor spreading. Journal of Geophysical Research 73, 3847–3858.
Stein, S., Okal, E.A., 2005. Speed and size of the Sumatra earthquake. Nature 434, 581–582.
Stein, S., Okal, E.A., 2007. Ultralong period seismic study of the December 2004 Indian Ocean earthquake and implications for regional tectonics and the subduction process. Bulletin of the Seismological Society of America 97, S279–S295. http://dx.doi.org/10.1785/0120050617.
Stein, C.A., Stein, S., 1992. A model for the global variation in oceanic depth and heat flow with lithospheric age. Nature 359, 123–129.

Suppe, J., 2007. Absolute fault and crustal strength from wedge tapers. Geology 35, 1127–1130. http://dx.doi.org/10.1130/G24053A.1.

Syracuse, E.M., van Keken, P.E., Abers, G.A., 2010. The global range of subduction zone thermal models. Physics of the Earth and Planetary Interiors 183, 73–90. http://dx.doi.org/10.1016/j.pepi.2010.02.004.

Tichelaar, B.W., Ruff, L.J., 1993. Depth of seismic coupling along subduction zones. Journal of Geophysical Research 98, 2017–2037.

Uyeda, S., Kanamori, H., 1979. Back-arc opening and the mode of subduction. Journal of Geophysical Research 84, 1049–1061.

Vigny, C., Socquet, A., Peyrat, S., Ruegg, J.-C., Métois, M., Madariaga, R., Morvan, S., Lancieri, M., Lacassin, R., Campos, J., Carrizo, D., Bejar-Pizarro, M., Barrientos, S., Armijo, R., Aranda, C., Valderas-Bermejo, M.-C., Ortega, I., Bondoux, F., Baize, S., Lyon-Caen, H., Pavez, A., Vilotte, J.P., Bevis, M., Brooks, B., Smalley, R., Parra, H., Baez, J.-C., Blanco, M., Cimbaro, S., Kendrick8§, E., 2011. The 2010 M_W 8.8 Maule Megathrust Earthquake of Central Chile, Monitored by GPS. Science 332, 1417–1421. http://dx.doi.org/10.1126/science.1204132.

von Huene, R., Ranero, C.R., 2003. Subduction erosion and basal friction along the sediment-starved convergent margin off Antofagasta, Chile. Journal of Geophysical Research 108, 2079. http://dx.doi.org/10.1029/2001JB001569.

Wallace, L.M., Beavan, J., McCaffrey, R., Darby, D., 2004. Subduction zone coupling and tectonic block rotations in the North Island, New Zealand. Journal of Geophysical Research 109, B12406. http://dx.doi.org/10.1029/2004JB003241.

Wallace, L.M., Reyners, M., Cochran, U., Bannister, S., Barnes, P.M., Berryman, K., Downes, G., Eberhart-Phillips, D., Fagereng, A., Ellis, S., Nicol, A., McCaffrey, R., Beavan, R.J., Henrys, S., Sutherland, R., Barker, D.H.N., Litchfield, N., Townend, J., Robinson, R., Bell, R., Wilson, K., Power, W., 2009. Characterizing the seismogenic zone of a major plate boundary subduction thrust: Hikurangi Margin, New Zealand. Geochemistry Geophysics Geosystems 10, Q10006. http://dx.doi.org/10.1029/2009GC002610.

Wang, K., Mulder, T., Rogers, G.C., Hyndman, R.D., 1995. Case for very low coupling stress on the Cascadia subduction fault. Journal of Geophysical Research 100, 12907–12918.

Wright, I.C., 1993. Pre-spread rifting and heterogeneous volcanism in the southern Havre Trough back-arc basin. Marine Geology 113, 179–200.

Wu, F.T., Kanamori, H., 1973. Source mechanism of February 4, 1965, Rat Island earthquake. Journal of Geophysical Research 78, 6082–6092.

Yagi, Y., 2004. Source rupture process of the 2003 Tokachi-oki earthquake determined by joint inversion of teleseismic body wave and strong ground motion data. Earth Planets Space 56, 311–316.

Zachariasen, J., Sieh, K., Taylor, F.W., Edwards, R.L., Hantoro, W.S., 1999. Submergence and uplift associated with the giant 1833 Sumatran subduction earthquake: evidence from coral microatolls. Journal of Geophysical Research 104, 895–919.